

Coastal processes modify projections of some climate-driven stressors in the California Current System

Samantha A. Siedlecki^{1*}, Darren Pilcher², Evan M. Howard³, Curtis Deutsch³, Parker MacCready³,
Emily L. Norton², Hartmut Frenzel³, Jan Newton⁴, Richard A. Feely⁵, Simone R. Alin⁵, and Terrie
Klinger⁶

¹Department of Marine Sciences, University of Connecticut, Groton, CT 06340, USA

²CICOES, University of Washington, Seattle, WA 98195, USA.

³School of Oceanography, University of Washington, Seattle, WA 98195, USA.

⁴Applied Physics Laboratory, Washington Ocean Acidification Center, University of Washington, Seattle, WA 98105, USA.

⁵NOAA Pacific Marine Environmental Lab (PMEL), Seattle, WA 98115, USA.

⁶School of Marine Environment and Affairs, Washington Ocean Acidification Center, University of Washington, Seattle, WA 98105, USA.

Correspondence to: Samantha Siedlecki (samantha.siedlecki@uconn.edu)

Abstract. Global projections for ocean conditions in 2100 predict that the North Pacific will experience some of the largest changes. Coastal processes that drive variability in the region can alter these projected changes, but are poorly resolved by global coarse resolution models. We quantify the degree to which local processes modify biogeochemical changes in the eastern boundary California Current System (CCS) using multi-model regionally downscaled climate projections of multiple climate-associated stressors (temperature, O₂, pH, saturation state (Ω), and CO₂). The downscaled projections predict changes consistent with the directional change from the global projections for the same emissions scenario. However, the magnitude and spatial variability of projected changes are modified in the downscaled projections for carbon variables. Future changes in pCO₂ and surface Ω are amplified while changes in pH and upper 200 meter Ω are dampened relative to the projected change in global models. Surface carbon variable changes are highly correlated to changes in DIC, pCO₂ changes over the upper 200 meters is correlated to TA, while changes at the bottom are correlated to DIC and nutrient changes. The correlations in these latter two regions suggest that future changes in carbon variables are influenced by nutrient cycling, changes in benthic/pelagic coupling and TA resolved by the downscaled projections. Within the CCS, differences in global and downscaled climate stressors are spatially variable, and the northern CCS experiences the most intense modification. These projected changes are consistent with continued reduction in source waters oxygen, increase in source water nutrients, and, combined with solubility-driven changes, altered future upwelled source waters in the CCS. The results presented here suggest projections that resolve coastal processes are necessary for adequate representation of the magnitude of projected change in carbon stressors in the CCS.

1 Introduction

Greenhouse gas emissions have imparted large physical and biogeochemical modifications on the world's oceans (Friedlingstein et al., 2019; Gattuso et al., 2015; Le Quéré et al., 2018). The oceans have become warmer and stratification

patterns have been modified (Talley et al., 2016). These changes are occurring in tandem with biogeochemical alterations, 35 including O₂ declines, productivity changes, and increased dissolved inorganic carbon content due to the uptake of anthropogenic carbon dioxide (Doney et al., 2009, 2020; Feely et al. 2004, 2009). The ocean uptake of anthropogenic carbon dioxide influences the ocean's buffering capacity, reduces calcium carbonate saturation states (Ω), and lowers pH causing a shift towards more acidity, commonly termed ocean acidification (Caldeira and Wickett, 2003; Doney et al., 2009; Feely et al., 2004, 2009; Orr et al., 2005; Sabine et al., 2004). These changing ocean conditions are occurring in both open-ocean and 40 coastal environments, where they have the potential to impact marine organisms and ecosystems individually (Doney et al., 2012, 2020; Gattuso et al., 2015) and as interactive multi stressors (Howard et al., 2020a; Portner et al., 2004; 2007). Big changes are happening in the ocean, but there are reasons to believe that global trends may not accurately represent what happens in coastal regions.

45 The majority of coastal areas have experienced significant increases in sea-surface temperature (SST) at a rate that exceeds the global average (Hartmann et al., 2013; Lima and Wethey, 2012). In contrast to most other large marine ecosystems, the coastal SST in the California Current System (CCS) has decreased over the past three decades (Lima and Wethey, 2012). These results suggest global projections and trends are poor indicators of future change in SST in the CCS and that spatial variability of that change within the CCS is also possible.

50

As the oceans warm, they lose O₂ because the solubility of O₂ decreases with increasing temperature. However, direct solubility effects only partially explain the O₂ decline (Bopp et al., 2013; Breitburg et al., 2018). Warming impacts O₂ in other ways, for example by raising organismal metabolic rates and accelerating O₂ consumption, and by increasing water column stratification and thus reducing mixing and ventilation (Breitburg et al., 2018; Deutsch et al., 2006). In coastal waters, hypoxic thresholds 55 are more often reached than in the open ocean because of eutrophication and other local processes, such as sediment O₂ demand (Diaz and Rosenberg, 2008; Rabalais et al., 2010; Siedlecki et al. 2015). In the CCS, hypoxia already occurs regularly on the continental shelf (Adams et al., 2013; Connolly et al., 2010; Chan et al., 2008; Grantham et al., 2004), and continental slope water O₂ concentrations have been steadily declining for the past several decades (Bograd et al. 2008; Chavez et al., 2017; Deutsch et al., 2011; 2014; Pierce et al., 2012).

60

Atmospheric carbon dioxide has increased at a rate of 1-2 ppm per year (Friedlingstein et al., 2019; Le Quéré et al., 2018), and surface waters in the open ocean have effectively kept pace with the rising atmospheric concentrations over the last 30 years. Recently, the partial pressure of carbon dioxide (pCO₂) in coastal shelf waters has been shown in some places to lag the rise in atmospheric CO₂, unlike in the open ocean, which implies a tendency for enhanced shelf uptake of atmospheric CO₂, with 65 substantial regional variability (Laruelle et al., 2018; Cai et al., 2020). One example of regional variability is found in the CCS: over the past 30 years, the CO₂ content of waters off the U.S. West Coast near Monterey Bay, CA, has increased at a rate greater than that observed in the open oceans (Chavez et al., 2017). As a result, surface water pH in Monterey Bay is on

average 0.01 units lower than surface open ocean measurements at the Hawaii Ocean Time-series due to the upwelling process, and is also declining at a slightly faster rate (Chavez et al., 2017). The enhanced uptake of CO₂ over the CCS shelf amplifies
70 the rate of acidification compared to global rates.

Local processes such as upwelling, freshwater delivery, eutrophication, water column metabolism, and sediment interactions drive biogeochemical variability on regional scales (Cai et al., 2011; Feely et al., 2008; 2016; 2018; Pilcher et al., 2018; Qi et
75 al., 2017; Siedlecki et al., 2017). In the CCS, winds are critical for upwelling variability and are projected to strengthen in response to global warming (Bakun, 1990; Garcia-Reyes et al., 2015; Wang et al., 2015; Rykaczewski et al., 2015; Sydeman et al., 2014). The increased delivery of O₂-depleted, carbon-rich waters, with enhanced nutrients and increased productivity has been projected for the CCS with a global simulation (Rykaczewski and Dunne, 2010). High-resolution projections for the CCS reinforced these findings (Dussin et al. 2019; Xiu et al., 2018), but projected that the impact of these altered conditions on productivity varied across the CCS with an increase in the north and a decrease in the south (Xiu et al., 2018), while
80 productivity was identified as driving the biggest change in hypoxia in the region (Dussin et al., 2019). Howard et al. (2020b) found that while alongshore winds intensified in the future, the upwelling response was damped by increased stratification. Global projections have coarse spatial resolution, often having only one or two grid cells for the continental shelf, and thus cannot resolve most of the local processes responsible for these observed coastal differences.

85 In this paper, we focus on the CCS and its known vulnerabilities to climate change by forcing regional models with the Coupled Model Intercomparison Project 5 (CMIP5, Taylor et al., 2012) simulations. We produce multi-model regionally downscaled climate projections of multiple climate-associated stressors (temperature, O₂, pH, Ω , and CO₂) that resolve coastal processes to create ~100-year projections at resolutions of 12-km and 1.5-km in the northern CCS (N-CCS). First, we quantify the surface to 200-meter depth averaged, sea surface, and bottom condition changes for the climate stressors projected for 2100 at all
90 resolutions (global, 12-km, and 1.5-km). Next, we use the multi-model ensemble to determine the degree to which climate associated stressors are modified relative to global model projections of the CCS considering this signal both spatially, where the models overlap, as well as in different regions of the water column representative of different habitats. Finally, we interpret our results in the context of previous projections for the CCS and suggest drivers of the amplification in the downscaled projections by systematically comparing the projected changes in the winds, source waters, upwelling strengths, and coastal
95 processes in each model system.

2 Materials and Methods

2.1 Model Descriptions

The downscaled regional modeling frameworks both employ the Regional Ocean Modeling System (ROMS, Shchepetkin and 100 McWilliams, 2005). The regional models are forced with realistic atmospheric and ocean boundary conditions to make hindcast simulations as well as future projections. The model domains are shown in Figure 1. The downscaled projections are referred to as “resolving coastal processes” because the historical simulations have been shown to represent observed coastal shelf variability. The model evaluation, provided here and available in other sources (Davis et al. 2014; Deutsch et al. in review; 105 Giddings et al. 2014; Siedlecki et al. 2015), indicate the downscaled models perform better spatially and temporally (seasonal and interannual) than the global models for temperature, oxygen and carbon variables.

~1-degree models: These include the CMIP model fields/global scale model. We focus here on only the representative concentration pathway 8.5 (RCP 8.5) from the Earth system models (ESMs) that make up the CMIP5 modeling framework. The CMIP5 simulations include biogeochemical components described in Bopp et al. (2013). The CMIP models employed here are further described in Section 2.3.

110 12-km model: The mid-resolution (12-km) ROMS-based simulation of the CCS is configured for a domain that extends along the North American west coast from 25 deg N to 60 deg N and described in more detail in Howard et al. (2020b). A curvilinear grid is used in the horizontal with close-to-uniform 12-km horizontal resolution and 33 s-coordinate (terrain-following vertical) levels. Atmospheric conditions including air-temperature at the sea surface, precipitation, and downwelling radiation are derived from an uncoupled Weather Research Forecast model output (c3.6.1; Skamarock et al. 2008) as in Renault, Hall, & 115 McWilliams (2016) and Renault et al. (2020) with more information in Howard et al (in review). To avoid the computational cost of a fully-coupled ocean-atmosphere model, wind and mesoscale current feedbacks are parameterized with a linear function of the surface wind stress as in Renault, Molemaker, et al. (2016). This linear relationship is supported by observations in the CCS (Renault et al. 2017). The biogeochemical model is detailed in Deutsch et al. (2020), and follows Moore et al. (2004). The model has skillfully simulated the recent interannual to interdecadal biogeochemical variability in the CCS 120 (Howard et al. 2020b), and a similar model setup forced with data-assimilated forcing skillfully simulated O₂ variability in the CCS over the last two decades (Durski et al., 2017).

125 1.5-km model: The highest resolution (1.5-km) simulations of the N-CCS rely on a modeling framework developed by the University of Washington Coastal Modeling Group optimized for the Pacific Northwest “Cascadia” region. The Cascadia model domain encompasses the inland waters of the Salish Sea, coastal waters of the N-CCS (Fig. 1), and includes freshwater and tidal forcing. The grid has a horizontal resolution of 1.5-km on the shelf, 4.5 km far offshore, and 40 s-coordinate (terrain-following vertical) levels, with enhanced bottom and surface resolution. The atmospheric conditions from the 12-km model are used to force the model at this resolution. The Cascadia model does not simulate biogeochemistry within the Salish Sea, but yields realistic nitrate outflow from the Strait of Juan de Fuca to the outer coast shelf (Davis et al., 2014). Hindcast experiments from 2004 to 2007 were extensively validated and exhibited skill on all regions of the shelf (Davis et al., 2014; 130 Giddings et al., 2014; Siedlecki et al., 2015).

2.2 Model Metrics

Carbon variables (e.g. pH, pCO₂, and Ω) were computed using model output of dissolved inorganic carbon (DIC), total alkalinity (TA), temperature, and salinity and routines based on the standard OCMIP carbonate chemistry adapted from earlier studies (Orr et al., 2005) using CO2SYS (Lewis and Wallace, 1998). The total pH scale is used for pH throughout.

135 To compute model means and inter-model comparisons, first a climatological year was generated for each model grid cell, using the 2002-2004 years for the 12km and 1.5km regional models. Then, annual average values for each cell were calculated from the climatology. Finally, spatially-weighted means were calculated from the annual average values. For comparisons between model resolutions, the coarser model was interpolated to the higher resolution model grid. For example, the global values were interpolated onto the 12-km grid prior to averaging the fields within the CCS. Surface conditions were drawn
140 from the surface vertical layer for each simulation. Depth-averaged ocean conditions were calculated over the upper 200 m for all simulations. Where water depth was shallower than 200 m, the entire water column was averaged. For the bottom comparisons, the global simulations have a very different bathymetry than the downscaled simulations because of their coarse resolution, consequently the regional averaging efforts reported here as bottom conditions were isolated to the 0-500 meters depth interval only, to ensure that the global model resolved that depth interval. We also report the downscaled values over
145 the shelf only, limiting the determination of metrics out to the 200 meter isobath.

Upwelling intensity – To estimate upwelling, several metrics were employed. The first two rely on the intensity of the winds (e.g. Cumulative Upwelling Index, CUI (Schwing et al., 1996); 8-day wind stress (Austin and Barth, 2002)), the third and fourth rely on measures in the water column itself and are referred to as the Coastal Upwelling Transport Index (CUTI) and
150 Biologically Effective Upwelling Transport Index (BEUTI) (Jacox et al., 2018). The wind-based metrics, CUI and the 8-day, are the same for both downscaled simulations, but CUTI and BEUTI are specific to each ocean model as they are calculated based on ocean measures like vertical transport and nitrate concentrations. CUTI and BEUTI were integrated over bins of 0.5-degree latitude spanning 0-50 km offshore.

2.3 Future Forcing

155 To generate future downscaled projections, the global CMIP5 simulations were used to force regional simulations. The methods employed are outlined below.

The 12-km historical simulation forcing is described in Renault et al (in review) and the companion paper, Deutsch et al. (in review). The 12-km projection was forced by adding a monthly climatological difference between CMIP5 RCP 8.5 scenario
160 forcing and the historical run forcing, averaged over 2071-2100 and 1971-2000, respectively (Howard et al., 2020b) following the delta method commonly applied in dynamical downscaling and described in Alexander et al. (2020). This is done for all variables that influence the surface energy budget including net downward shortwave and longwave radiation, 10-m wind

speed (u and v component), air temperature, and specific humidity. CMIP5 models are from GFDL (ESM2M), IPSL (CM5A-LR), Hadley (GEM2-ES), MPI (ESM-LR), NCAR (CESM1(BGC)). A total of six RCP 8.5 scenario runs were conducted: 165 one for each individual CMIP5 model realization, and a final run using the five-member ensemble mean forcing. For this manuscript, we report the output from this final, ensemble mean-forced scenario. However, the output from the five individual CMIP5 model realizations were used to calculate the standard deviation values across the ensemble spread reported in Table 1. Initial and boundary conditions had the same kind of centennial trend addition for temperature, salinity, and all 170 biogeochemical tracers (O₂, nitrate, phosphate, silica, iron, dissolved inorganic carbon, alkalinity). More information can be found in Howard et al. (2020b, Table 1).

The 1.5-km projection was forced using the open ocean boundary conditions and atmospheric forcing from the 12-km regional simulation described above (Howard et al., 2020b). The boundary conditions included biogeochemical fields from the 12-km model. Because the ecosystem model (BEC) in the 12-km parent grid has more variables than the Cascadia simulation, some 175 of the variables were merged. Specifically, the phytoplankton fields were added together, and the nutrients (ammonia and nitrate) were summed into one nitrogen field. To ensure no biogeochemical model drift between the nested 1.5-km simulation and the 12-km simulation, after one year of spin up, a simulation of 2007 was compared against observations from the region (Fig. 2). The 1.5-km biogeochemical model skill was similar to the original model runs previously published (Davis et al. 2014; Giddings et al. 2014; Siedlecki et al. 2015) for 2007 (Fig. 2) without any significant drift in time. Temperature and 180 salinity both experienced a significant bias in the upper 200 meters in this configuration, unlike the previously published model runs (Fig. 2; temperature RMSE 2.43; salinity RMSE 0.627). As we are focused on differences between the modern and the future and we expect the bias to remain the same, we do not bias correct the forcing here.

For the future conditions, atmospheric CO₂ concentration (800 ppm), and future atmosphere and ocean forcing from the 12- 185 km runs drove the Cascadia simulations. The river forcing was approximated by altering the timing of the freshet of the 2007 forcing earlier in the year by two months. This is in line with some historical analyses from the N-CCS region (Riche et al., 2014) as well as some projections of future hydrological conditions for the Fraser River (Morrison et al., 2002). Both of these results suggest that the total precipitation will remain the same, but the increase of rain and decrease in snowpack will shift the freshet earlier (Figure S2). The river TA was not altered from historical forcing, but the rivers equilibrate with the future 190 atmospheric CO₂ concentration (800 ppm).

2.4 Future Change

For each resolution, simulations were run for a number of years in a base/present state and then compared to a future simulation. The change is the difference between the future and base/present state, representing a ~100-year anomaly due to climate forcing. The historical/base state for the CMIP5 runs was computed from an ensemble mean spanning 1971-2000. For the 12- 195 km simulation, the base/present state spanned 1994-2007. For the 1.5-km simulation, the model was spun up for one year

(2001) and then the base/present state spanned 2002-2004. Each level of resolution entails additional computer resource costs, which is part of the appeal of large-scale simulations. The CMIP5 future runs consist of a thirty-year mean spanning 2071-2100. The 12-km model is a late 21st century run spanning 2085-2100. The 1.5-km model is also late 21st century spanning 2094-2096. Results and comparisons for the work presented using both the 12- and 1.5-km-resolution simulations were made 200 using the same year span despite runs existing for a broader range of years for the 12-km simulation. The present state was considered as 2002-2004 for both the 12 and 1.5-km simulations and the future was 2094-2096 (Table 1). The global model ensemble average results represent a 30 year climatology.

2.5 Modification

The range of the five ensemble members which forced the 12-km projections is used to bound the potential futures expected. 205 When the differences provided in Table 1 between the mean downscaled conditions for a region of the CCS (CCS-wide, columns B-C or Cascadia/N-CCS, columns E-G) and the ensemble spread quantified from the 12-km model projections (columns D and H) both exceed the 1 degree model projected change (columns B and E), those regions of the CCS are projected to undergo amplified change. The converse is referred to as dampening. The ensemble spread is provided in Table 1 as the 210 range of the 5-member model spread of the annual average results for the 12-km model projections (columns D and H). The direction with which each variable described above was amplified relative to the global models is highlighted using dark grey (amplified) and light grey (dampened) shading in Table 1.

3 Results

Model projections of climate-driven stressor variables (temperature, O₂, pH, saturation state (Ω), and CO₂) in each downscaled projection were compiled for the CCS for three depths (200 m averaged, surface, and bottom < 500 m; Table 1; Fig. 3-5). The 215 global average changes for many of these variables are different from the 1 degree model projected values for the CCS region, but in only a few cases does this difference fall outside of the ensemble spread reported in column D and H of Table 1 (i.e., the signal is amplified or dampened). For each variable and depth, the change between the base state and the projected state is described below and evaluated within the context of the ensemble spread.

3.1 Temperature

220 The surface to 200-meter depth-averaged temperatures at all model resolutions is consistently warmer in the future CCS, both CCS-wide (1.63 and 1.81 degrees C in the 1 degree and 12-km models, respectively, Table 1, columns B and C), and within the N-CCS (1.95 to 2.32 degrees C across the three model resolutions; Figure 3a; Table 1 Columns E-G). The Washington shelf experiences the largest projected differences in the 1.5-km projection (2.32 degrees C, Fig. 3). The 1-degree model projected increase for the CCS (1.63 degrees C) and the N-CCS (2.21 degrees C) falls within the range of warming from the

225 downscaled projections (CCS: 1.38 to 2.24 degrees C; N-CCS: 1.55 to 2.35 degrees C, Columns D and H in Table 1). In both regions of the CCS, the differences between the models are smaller than the range of the 12-km ensemble (Table 1).

At the surface, the SST is warmer in the future in all projections. Spatially, the SST increases most offshore, and increases least near the coast in all simulations of this eastern boundary upwelling system, as a result of upwelling (Fig. 3b). The 1.5 km
230 model projects slightly smaller increases in SST than the 1-degree model or the 12-km model. However, the 1-degree models project SST increases CCS-wide (3.12 degrees C) and in the N-CCS (3.15 degrees C), which fall within the range of SST projections from the 12-km ensemble of downscaled projections (CCS: 2.57 to 4.05 degrees C; N-CCS: 2.42 to 4.18 degrees C, Columns D and H in Table 1).

235 At the bottom, the temperature increases the most near the coast. The abyssal regions show little to no change in temperature (Fig. 3c). The shallowest regions of the 1.5-km simulation experience the largest warming - nearly 3 degrees C. In the coastal process-resolving downscaled projections, the projected bottom temperature change is greater (1.75-1.84 degrees C, 2.05 degrees C) than the global projections (1.34-1.65 degrees C). However, the 1-degree model projected increases for the whole CCS (1.65 degrees C) fall within the range of temperature projections from the ensemble of 12-km projections (CCS: 1.47 to
240 2.21 degrees C, Column D in Table 1), while the N-CCS (1.34 degrees C) is lower than the range of temperature projections from the ensemble of 12-km projections (N-CCS: 1.40 to 2.10 degrees C, Columns H in Table 1).

3.2 Oxygen

Annual depth-averaged O₂ concentrations at all model resolutions consistently decrease in the future compared with the base state, but the magnitude of the decrease is slightly more severe on average in the downscaled projections (Table 1; Fig. 3). The
245 spatial variability within the CCS region, with more severe declines occurring in the N-CCS, is consistent across models but varies in magnitude. The 1-degree model projected decrease for the CCS (-0.52 ml/l) and the N-CCS (-0.56 ml/l) fall within the range of the ensemble of projections from the 12-km model (Table 1; CCS: -0.52 to -0.72 ml/l; N-CCS: -0.52 to -0.92 ml/l, Columns D and H in Table 1).

250 At the surface, O₂ declines in all projections, and the degree of change is similar across resolutions (Table 1; Fig. 3) consistent with the solubility effect from surface temperatures in each simulation. The 1-degree model projected decline falls within the spread ensemble of projections from the 12-km model for the CCS.

The bottom O₂ concentration declines in all projections near the coast (Table 1; Fig. 3). The range of change in bottom O₂ on
255 the shelf in the 1.5-km projection varies by a factor of two, with the most extreme changes occurring on the outer shelf and in pockets known to experience persistent hypoxia in the present ocean - e.g. near Cape Elizabeth, south of Heceta Bank, and within the region associated with the Juan de Fuca Eddy (Siedlecki et al., 2015). The 1 degree model projected decrease for

the CCS (-0.43 ml/l) and the N-CCS (-0.63 ml/l) falls within the ensemble range of the ensemble of bottom O₂ concentration projections from the 12-km model (CCS: -0.37 to -0.75 ml/l; N-CCS: -0.40 to -0.92 ml/l, Columns D and H in Table 1). When
260 the bottom is restricted to the shelf in the downscaled simulations (< 200 m isobath; values with asterisk (*) in Table 1), this decrease is more severe but still does not fall outside the range from the comparable depth range of the 1-degree model projection (<500 m).

3.3 pCO₂

All model projections of pCO₂ consistently increase, with larger increases in the downscaled projections than in the global
265 projection (Table 1; Fig. 4). The spatial variability within the CCS region differs across resolutions. All projections show an onshore-offshore gradient in pCO₂ with smaller changes closer to the coast and larger changes offshore. In the coastal process-resolving downscaled projections, the projected depth-averaged change in pCO₂ increases, and the gradient between the nearshore and offshore intensifies. The 1-degree model projected increase for the CCS (492 μ atm) and the N-CCS (527 μ atm) falls below the ensemble range of downscaled pCO₂ projections from the 12-km model (CCS: 682-836 μ atm; N-CCS: 780 to
270 1066 μ atm, Columns D and H in Table 1).

At the surface, future pCO₂ consistently increases in all projections, but varies widely across resolutions (Table 1; Fig. 4). In the downscaled projections, most upwelling areas experience a smaller increase in surface pCO₂ than offshore waters. In the
275 1.5-km projection, regions near the coast of Oregon show the largest surface pCO₂ differences between the base and future states, while the region associated with the Columbia River plume shows a much smaller change. Overall, the inclusion of coastal processes contributes to the spatial patterns and magnitudes of projected changes. Consistent with the subsurface signal, the 1-degree model projected increase for the CCS (392 μ atm) and the N-CCS (365 μ atm) fall below the ensemble range of the downscaled projections from the 12-km model (CCS: 433 to 437 μ atm; N-CCS: 424 to 434 μ atm).

280 At the bottom, pCO₂ is consistently higher in all projections, with varying magnitude across the model resolutions (Table 1; Fig. 4). The range of change in bottom pCO₂ on the shelf of the 1.5-km projection varies widely (600-1200 μ atm), with the most extreme changes occurring on the outer shelf and in pockets known to experience persistent hypoxia at present. The 1-degree model projected change for the CCS (505 μ atm) and the N-CCS (592 μ atm) fall below the ensemble range of projections from the 12-km downscaled model (CCS: 650 to 920 μ atm; N-CCS: 776 to 1154 μ atm).

285 3.4 pH

The pH averaged over 200-meter depths for all model resolutions consistently decreases, and change is less severe than the global models project for the CCS region (Table 1; Fig. 4). In the 12-km simulation, a slightly smaller pH change (~ -0.26) is observed in the southern CCS than the entire CCS, within the influence of coastal upwelling. In the 1.5-km simulation, the regions of largest decline are on the outer shelf and patches of the Oregon shelf. In the downscaled projections, the depth-

290 averaged 200-meter pH is lower than the 1-degree model projected change in the North and greater than the global change CCS -wide. The 1-degree model projected decrease for the CCS (-0.321) and the N-CCS (-0.332) fall within the ensemble range of projections for the downscaled 12-km model (CCS: -0.310 to -0.357; N-CCS: -0.278 to -0.352).

295 At the surface, the pH consistently decreases in all projections, and is less severe a decrease in the downscaled projections than for the same region in the global model (Table 1; Fig. 4). The 1-degree model projected decrease for the CCS (-0.319) and the N-CCS (-0.343) is larger than the ensemble range of projections for the downscaled 12-km model (CCS: -0.285 to -0.287; N-CCS: -0.296 to -0.300).

300 At the bottom, the pH decreases on the shelf in all projections (Table 1; Fig. 4). In the 1.5-km resolution model, the projected conditions show spatial variability on the shelf that is not apparent in the coarser models. The most severe changes in bottom pH correspond with regions that experience the largest changes in bottom O₂. The downscaled projections indicate decreases in annual average bottom (< 500 m) pH, but spatial variability exists on the shelves in the coastal process-resolving simulations. This difference between the 1 degree and downscaled simulations is even greater on the shelves (indicated as the starred values in Table 1). The 1-degree model projected decline for the CCS (-0.286) falls within the ensemble range for the downscaled 305 12-km model (CCS: -0.228 to -0.290) while the N-CCS 1-degree model projection (-0.333) is larger than the ensemble range of projections (N-CCS: -0.230 to -0.312) for the downscaled 12-km model.

3.5 Ω

310 Projections of Ω_{arag} and Ω_{calcite} averaged over 200 m depths at all model resolutions consistently decrease in the future, but the magnitude of decrease is usually greater in the downscaled projections (Table 1; Fig. 5). The projected difference is greater on the shelf than offshore, but this gradient is weaker in the 1.5-km projection. The 1 degree model projected decline in Ω_{arag} for the CCS (-0.71) falls within the ensemble range of projections for the downscaled 12-km model for the CCS (-0.65 to -0.75). The 1 degree projected decline in Ω_{arag} for the N-CCS (-0.62) is larger than the ensemble range of projections and larger than the ensemble range of projections for the N-CCS (-0.41 to -0.53) in the downscaled 12-km model. The same patterns are true for the Ω_{calcite} averaged over 200 m depths (Table 1).

315

At the surface, Ω consistently decreases in all projections (Table 1; Fig. 5). Spatially, the 12-km projection shows the largest declines in surface Ω in the southern domain with little gradient between the shelf and offshore. At the 1.5-km resolution, the N-CCS projected declines are lowest offshore, and the declines are even larger than the 12-km projected changes even when considering the ensemble spread. The 1-degree projected decrease for the CCS (-0.96) is larger than the range of the ensemble 320 of projections from the downscaled 12-km model (CCS: -0.86 to -0.94). The 1 degree projected decrease for the N-CCS (-0.76) is smaller or less severe than the range of the ensemble of projections from the downscaled 12-km model (N-CCS: -0.82 to -0.88). The same is true for the surface decline Ω_{calcite} (Table 1).

At the bottom, Ω decreases in all projections near the coast on the shelves (Table 1; Fig. 5). At the 1.5-km resolution, spatial
325 variability in the magnitude of the projected conditions exists on the shelf. The most severe changes in bottom Ω correspond
with regions that experience the largest changes in bottom O_2 . In the N-CCS, the 1.5-km projected declines are even larger
than the 12-km projected declines even when considering the ensemble range. The 1-degree model projected decline in Ω_{arag}
for the CCS (-0.47) is more severe than the downscaled ensemble range (CCS: -0.38 to -0.46) for the downscaled 12-km model.
In the N-CCS, the 1-degree model projected decline in Ω_{arag} for the N-CCS (-0.32) falls within the range of the ensemble of
330 projections from the downscaled 12-km model (-0.30 to -0.40). In the 1.5-km model projections, the decline is greater than the
1-degree model projects and falls well outside the range of the 12-km projections. This difference between the global and
downscaled simulations is even greater on the shelves (indicated as the starred values in Table 1). The same is true for the
bottom decline in Ω_{calcite} (Table 1).

335 **3.6 Themes across projected changes for the CCS**

All climate-associated stressor variables agree with the 1-degree projections in terms of the direction of the trend, but not the
magnitude of the change. The 1-degree model projections for the CCS are largely consistent with the 1 degree model projected
global trends with some differences in the nearshore upwelling areas (Fig. S1). All carbon variables are sensitive to the
inclusion of coastal processes which both downscaled projections provide. In addition, all of the projections suggest greater
340 change in most variables in northern regions of the CCS, and in the upwelling regions.

Nitrate increases over much of the domain in the upper 200 m (Fig. 6, Table S1) in both the high- and medium-resolution
downscaled simulations. Nitrate on average increases in the global simulations, but the magnitude and direction varies widely
across the ensemble members, a result consistent with Howard et al. (2020b). In addition to the projected small increase in
345 nutrient concentrations in the upwelling system of the CCS, the winds are slightly more intense (2 % increase in the magnitude
of the wind stress) during the upwelling season (April - September) in the future years. The timing of the onset and duration
of the upwelling season in the northern CCS remains the same in the future in these projections. Despite these differences
from wind-based upwelling metrics, the in-water upwelling metric CUTI indicates no net change in the upwelling intensity of
350 the future N-CCS in the simulations evaluated here. When nitrate is included in the upwelling measure, as in BEUTI, there is
a slight decline in the upwelling of nitrate (1-2%), consistent with a decrease in nitrate at the surface in the N-CCS (Fig. 6).
This result is sensitive to the distance offshore (20-75km) over which the index is calculated. The direction of the trend does
not change, but BEUTI for example, further declines (4%) as bin boundaries move closer to shore. The further offshore the
bin extends, the weaker the signal becomes. Both of these measures suggest that the upwelling is not intensified in our
355 projected future, despite the slight increase in winds. This result is consistent with the results of Howard et al. (2020b), where
increased stratification in the future simulations impeded increases in upwelling intensity.

The projected temperature change affects the solubility of the gases, generating a solubility-driven decline, and the increased nutrient content would correspond to a stoichiometric oxygen loss as well. Over the entire CCS, the decrease in oxygen over the upper 200 meters was 0.45 ml/l or 20.10 mmol/m³ (Table 1). The solubility-driven change accounts for most (~67%) of
360 this change (13.42 mmol/m³ using 1.92 change in temperature from Table 1). The additional nitrate brought into the region from the large-scale models (0.79 mmol/m³) corresponds to an additional drawdown of 6.81 mmol/m³ of oxygen. In the N-CCS, the change in oxygen is a bit larger than across the entire CCS – 0.69 ml/l (30.82 mmol/m³, Table 1). The solubility driven changes contribute a bit less (~44%) in the N-CCS than the entire CCS, but the nitrate signal is larger in the N-CCS
365 corresponding to 11.21 mmol/m³ change in oxygen from an increase of 1.3 mmol/m³ of nitrate in the upper 200 meters of the water column. The result is that the solubility driven changes combined with the increased supply of nutrients to the upper 200 meters of the N-CCS account for 80% of the projected oxygen change in the N-CCS.

Similarly, we would expect carbon content to increase in source waters commensurate with an increase in nutrients and lower oxygen concentrations. The corresponding stoichiometric increase in DIC to the increase in nutrients (5 mmol/m³) would only
370 account for a small decline in pH (0.02) or Ω (0.03). The majority of the pH and Ω decline is due to anthropogenic carbon content increase in DIC associated with the RCP 8.5 scenario forcing (~95 mmol/m³). Spatial variability in Δ DIC corresponds with variability in the water buffer capacity and Revelle factor, with southern CCS regions of relatively high buffer capacity having the greatest rates of DIC uptake (Fig. 7, Table S1).

375 TA increases in the future in the subsurface on the shelves of the CCS and even more so on the upper slope (Fig. 7, Table S1), but it mostly decreases across domains. At the surface, it declines, and these two changes offset each other in the depth-averaged 200 meter change. Overall, the projections from the downscaled simulations decrease in TA is substantially smaller than the decrease from the 1 degree models (Table S1). These changes in their corresponding depth ranges contribute to the
380 results for the carbon variables in Table 1, impacting different carbon variables differently, for example, pCO₂ is amplified while pH is not modified over much of the CCS, and Ω is amplified at the bottom and the surface but damped over the upper water column. These patterns will be examined more closely in Section 3.7 that focuses on modification and which follows.

On the shelves of the downscaled simulations, the source waters are further modified by coastal processes including increased
385 benthic-pelagic coupling, freshwater delivery and denitrification. The inclusion of these processes causes the bottom waters on the shelf to experience a more severe increase in pCO₂ and declines in oxygen, pH, and Ω than observed in the shallowest regions of the global models (starred values in Table 1). The difference between the bottom estimated changes in the CCS in the depth ranges resolved by the global models and on the downscaled shelves is greatest for the carbon variables.

3.7 Modification

In general, the CCS experiences a greater change for most variables at all resolutions than the global ocean. However, only
390 the carbon variables emerge as amplified or dampened by the downscaled simulations. Across the spread of ensemble members
for the entire CCS in the 12km simulation, the downscaled projected increase for pCO₂ (columns C, F, G) is amplified relative
to the 1-degree models (columns B, E) in all three depth ranges (Table 1). The N-CCS pCO₂ increase is amplified in both
downscaled simulations (12-km, 1.5km), at all depth ranges (Table 1, columns F and G). In the 200 m depth averaged changes,
395 the pCO₂ change is correlated to the TA changes (Table S2). At the surface the changes in pCO₂ are correlated to the
temperature, and at the bottom, DIC, TA, and nutrient changes (Table S2).

The downscaled decrease in pH at the surface and the bottom is modified relative to what the 1-degree models project for the
CCS and N-CCS in the downscaled projections. The surface change is less severe than in the 1-degree model, and so is
400 considered dampened relative to global change. At the bottom, pH in the N-CCS is dampened relative to the 1-degree model.
In both downscaled projections (12-km, 1.5km), the surface and bottom pH decrease is dampened in the N-CCS relative to the
surface pH decline in the 1 degree model for that region (column E). While pH is not modified in the 200 m depth averaged
changes, at the surface, the pH changes are correlated to the DIC and TA (Table S2).

The decrease in Ω over the upper 200 meters is less severe than the 1-degree model projection for the N-CCS, and falls outside
405 of the ensemble range, so is considered dampened relative to global change (Table 1). The N-CCS 200 m depth averaged Ω
decrease is dampened in both downscaled simulations (12-km, 1.5km), and amplified at the surface (Table 1). At the surface,
the changes in saturation state are highly correlated to DIC changes. At the bottom, the changes are also correlated to the
changes in nutrients (Table S2). In the N-CCS region, more of the water column is modified for the carbon variables.

4 Discussion

410 Globally, under RCP 8.5, the future oceans simulated using CMIP5 are projected on average to be warmer (SST, mean \pm 1
SD: $2.73 \pm 0.72^\circ\text{C}$), higher in pCO₂, lower in O₂ content (RCP8.5: $-3.45 \pm 0.44\%$), and more acidified (surface pH $-0.33 \pm$
0.003 units) (Gattuso et al., 2015). Regionally, the CMIP5 models project the North Pacific to be one of the regions to
experience the most warming, most severe O₂ declines, and largest extents of corrosive conditions (Bopp et al., 2013; Feely et
415 al., 2009; Gattuso et al., 2015; Gruber et al., 2012; Hauri et al., 2013; Long et al., 2016). Here, we present one of the first
downscaled multivariable projections of environmental change out to the end of the century in the CCS driven by a suite of
CMIP5 forcings instead of a single global model. While the downscaled projections show changes that are similar in direction
to those of the global simulation, the magnitude and spatial variability of the change differs in the coastal process-resolving
downscaled projections and to a varying degree depending on the variable, depth range, and subregion of interest.

420 The CCS experiences a greater change for many variables at all resolutions than the global ocean, however this change is modified in the CCS in both downscaled simulations (12-km, 1.5km), for $p\text{CO}_2$, Ω_{arag} and Ω_{calcite} , and pH. Amplification of global trends within the CCS upwelling systems in the future has been shown before for oxygen specifically (Dussin et al., 2019) and was identified through the response of the downscaled model to a series of idealized experiments with perturbations in the source water oxygen and nutrient concentrations. Source water changes in oxygen drove a two-fold larger change in
425 oxygen than nutrient supply alone, and both of these drivers were determined to be more important than intensifying winds. In our projections, the more realistic winds were different than in Dussin et al. (2019), with a small intensification of about 2%. The source waters were lower, but the oxygen decrease in the N-CCS fell within the range of the ensemble members explored here. Dussin et al. (2019) only explored one global model (GFDL) as a driver, and as such the definition of amplification differs from the one we use here. Much like experiments conducted by Liu et al. (2012, 2015) for ocean
430 temperatures and described in Alexander et al. (2020), using a multi-model mean to drive a downscaled ocean model retains the linear component of the climate change forcing only and is not able to assess the range of the response. Fundamentally, our definition of amplification relies on the range of the ocean condition responses. The mechanism of remote biogeochemical redistribution and influence via boundary conditions in the CCS remains influential for the carbon variables that were identified as amplified here. While climate stressor variables have been identified as amplified historically using records spanning
435 several decades or more (Chavez et al., 2017; Osbourne et al., 2020), regional future projections have focused on multi-model mean conditions projected over 100 years into the future.

Although the downscaled model projected a small intensification in the projected upwelling-favorable wind stress of 2% which is consistent with prior work on this topic (Bakun, 1990; Garcia-Reyes et al., 2015; Rykaczewski and Dunne, 2010; 440 Rykaczewski et al., 2015), no change was quantified in the upwelling fluxes in the water column using the CUTI, and a slight decline was observed in BEUTI (nutrient flux) measures of upwelling. This is likely due to the compensation from increasing stratification in the future simulations as noted in Evans et al. (2020). We observe lower oxygen, higher nutrient content in source waters, but this change does not make it to the surface. Within the CCS, solubility-driven oxygen changes are important, which is consistent with oxygen escape from the ocean being increasingly important in future projections (Li et al. 2020).
445 Moving south within the CCS, solubility increasingly outcompetes nutrient-driven changes in oxygen drawdown. However, the projections here indicate that the magnitude of oxygen decrease was within the bounds of the ensemble range, and so was not amplified relative to the global models, unlike the carbon variables.

The projected change in pH is consistent with prior pH projections for the CCS downscaled with the same RCP 8.5 scenario 450 using a ROMS model (Gruber et al., 2012; Hauri et al., 2013; Marshall et al., 2017; Turi et al., 2016). These projections were performed with different biogeochemical models described in Gruber et al. (2012), and Fennel et al. (2006, 2008) and relied on multi-model means or individual ensemble members for the global models. The pH values we obtained are lower than the projections of Rykaczewski and Dunne (2010) for the CCS. They used GFDL Earth System Model 2.1, a different forcing

scenario, and a different biogeochemistry model (Dunne et al., 2007). Despite clear modification of global trends indicated by 455 downscaled projections provided here of pCO_2 , Ω , and pH, the biogeochemical model formulations differ across resolutions and may be contributing to the amplified signals. Differences include parameterizations of gas exchange, detritus classes, sinking velocities, as well as benthic boundary conditions; the latter has been identified in prior work to be important for O_2 models in coastal regions (Moriarty et al., 2018; Siedlecki et al., 2015). Any of these could contribute to the differences observed across model resolutions. CMIP5 results are based on an ensemble average of many models, which all utilize different 460 formulations and complexities for their ecosystem models, further contributing to the uncertainty provided from the biogeochemical boundary conditions. Overall, the projected annual, depth-averaged change in pH appears to depend mostly on the anthropogenic forcing scenario, and all the models agree on the direction and relative magnitude despite these differences.

465 Projected changes in surface and bottom pH, Ω , and pCO_2 are modified by the inclusion of coastal processes when downscaling is employed. Coastal processes that influence the variability of carbon variables occur in these regions of the water column include freshwater delivery and sediment water interactions. At the surface, pH, Ω and pCO_2 change differently. TA declines at the surface, while DIC increases. DIC increases due to increased storage of carbon from the increase in carbon in the future atmosphere. The TA changes are driven in part by the altered timing of the freshet in the N-CCS as well as the presence of a 470 river plume in an upwelling regime. Freshwater in the region is known to be corrosive due to naturally low TA, which impacts the buffering capacity of the surface waters. This result can be seen in the surface difference plots for pCO_2 near the Columbia River plume (Fig. 4) and the surface TA change (Fig. 7). The 12-km projections include climatological freshwater fluxes as precipitation along the coastline instead of resolving river plumes like the 1.5-km projections, but despite these different freshwater parameterizations, both models indicate modification of carbon variables in the N-CCS Cascadia domain with 475 different directions for different variables. While the freshwater amplifies the global rate of change for the surface pCO_2 and Ω , over the entire water column (200 m average), the pH change is damped as the DIC and TA changes are offset by the temperature changes for that variable.

In our regional downscaled simulations, the change in temperature and TA act together to offset the increase in the DIC signal 480 in the coastal upwelling regime (Fig. 7), and for pH these changes offset each other in the upper 200 m of the water column. The global models show very little change in TA in the region. While the downscaled bottom TA change is small (20-50 mmol/m³, Fig. 7, Table S1), this amounts to an increase in pH of 0.07-0.18 and an increase in Ω of 0.15-0.21 - enough to offset 40-60% of the reduction in Ω due to increased atmospheric CO_2 concentrations. At the bottom, the increase in TA modifies the projected pH change in the N-CCS by reducing it.

485

Both biogeochemical models include denitrification at the sediment water interface which impacts both the nitrogen and TA cycling in the model. Denitrification is a source of TA (Chen et al., 2002) and has been shown to impact shelf wide TA in

other regions (Fennel et al., 2008). In the CCS, denitrification has been observed on the shelf and slope, peaks on the slope, and is greater off the Washington coast than off Mexico (Hartnett and Devol, 2003). As the source waters become lower in 490 oxygen content, denitrification should increase, providing an additional feedback on the nutrients and carbon variables, and dampening the global ocean acidification signal. Bottom Ω is not amplified in Table 1, but if calculated solely over the shelf region (asterisks in Table 1), then bottom Ω changes are amplified in both domains. While this source of alkalinity has not been observed directly in the modern ocean, a source of TA was identified and interpreted as calcium carbonate dissolution in 495 the CCS (Fassbender et al., 2011). These results suggest future projections should consider salinity and TA forcing feedbacks when performing regional projections as these can alter regional impacts of carbon variables.

Different carbon variables are sensitive to different physical climate forcings, a result that is consistent with recent work suggesting that competing sensitivities may dampen the variability of pH in the future (Jiang et al., 2019; Kwiatkowski and Orr, 2018; Salisbury and Jonsson, 2018; Takahashi et al., 2014). The sensitivities of the various carbon variables to thermal 500 and geochemical (carbon dioxide) forcing was explored in an idealized simulation of future conditions from CMIP5 models in Kwiatkowski and Orr (2018), in the modern ocean in Takahashi et al. (2014) and Jiang et al. (2019), and in the Gulf of Maine by Salisbury and Jonsson (2018). Kwiatkowski and Orr (2018) determined that the balance between the change in DIC and TA drives the variability of pH, in combination with temperature in mid-to-high latitudes -- effects that largely cancel each 505 other out. While the processes that control TA and DIC are similar, the addition of atmospheric CO₂ changes DIC alone, altering the balance between these two reservoirs. In the Gulf of Maine, temperature and salinity anomalies in combination with TA variability offset the long-term OA trend (Salisbury and Jonsson, 2018). Their analysis indicated that Ω is more sensitive to temperature and salinity variations than pH, and this result was confirmed globally in Jiang et al. (2019). Kwiatkowski and Orr (2018) also found the seasonal amplitude of Ω_{arag} is expected to strengthen in some regions and attenuate in others due to the high sensitivity of this variable to temperature.

510 By examining the relationships between the carbon variables and other regional variables, the relative importance of different processes responsible for the modification of carbon variables by coastal systems can be inferred. Themes emerge in the correlations with carbon variables across different regions of the water column: at the surface, DIC changes are important, and at the bottom, changes in DIC, TA, and nutrient content changes have the highest correlations with more than one carbon 515 variable. Over the 200 m water column, TA is important. The TA decreases in all the projections but by an order of magnitude less than the 1 degree models in the downscaled simulations (Table S1). A dampened reduction in TA is consistent with changes in the biological metabolism or benthic pelagic coupling alongside the sedimentary processes in the region - all of which can act as a source of TA on shelves.

520 If we take a specific example of Ω , the Ω changes are correlated with nutrient content changes, in addition to the DIC changes that result from the emissions scenario forcing. As a result, bottom Ω on the shelf is modified by the TA generation organic

matter remineralization and via sedimentary processes. Consistent with this result, the bottom change in DIC is greater in the downscaled simulations than the 1 degree models (Table S1). The 1 degree models do not resolve the shelf bathymetry, and thus the sedimentary processes that seem likely to play an important role in this coastal setting.

525

These results are consistent with the idea that the changes in different regions of the water column are driven by different mechanisms - surface changes in the carbon variables are driven by the RCP and modified by coastal biological cycles, bottom conditions are influenced more by benthic pelagic coupling and sedimentary processing as suggested by the TA and nutrients correlations, and the water column modification is a combination of all of these.

530

Spatially, within the CCS, the projections suggest greater change in most variables in northern regions of the CCS, and on the shelves in the annual averages. Currently, the N-CCS is the most productive region of the CCS (Davis et al., 2014; Hickey and Banas, 2008) and experiences the most prevalent hypoxia (Connolly et al., 2010; Peterson et al., 2013) and corrosive events (Feely et al., 2018; 2016). One aspect that differentiates the region from the rest of the CCS is that the N-CCS experiences 535 both seasonal upwelling and downwelling currently (Hickey and Banas, 2008), which is not projected to change in 2100 under RCP8.5. During the summer upwelling season in the N-CCS, oxygen declines on the shelf over the season as organic material and respiration increases on the shelf. Coincident with the oxygen decline, carbon parameters are impacted in kind (e.g. pH and Ω decreases, pCO_2 increases; Siedlecki et al. 2016; Feely et al. 2018). The dramatic fall transition on the Washington and Oregon shelves is observed in the modern ocean (Adams et al. 2013; Connolly et al. 2011; Hales et al. 2006; Siedlecki et al. 540 2015), fully quantified by an oxygen budget in Siedlecki et al. (2015), and is projected to continue in the future projections examined here. The continued existence of a downwelling season in the future impacts some variables more than others. The projected change for oxygen and carbon variables is different seasonally. The fall transition and winter mixing re-oxygenates shelf waters (Siedlecki et al., 2015), and this pattern continues into the future. Hypoxia will continue to exist in the summer months, but for a longer period of the summer. Corrosive, low pH conditions, however, will occur year-round. The fraction of 545 the year during which bottom water on the shelf is corrosive ($\Omega < 1$) or low pH ($pH < 7.65$) nearly doubles. This asymmetry has been identified previously in the Salish Sea (Ianson et al., 2016), and exists because of the difference in equilibration timescales at the surface for oxygen and carbon dioxide.

5 Conclusions

We present one of the first multi-model, downscaled multivariable projections of changing temperature, pH, pCO_2 , Ω , and O_2 550 in the CCS. The downscaled projections are driven by the same delta forcing as the global simulation, and projected changes for the CCS are consistent with the directional trends indicated by the global model for scenario RCP 8.5 - warmer, more acidified, higher carbon content, and lower oxygen concentration. However, the magnitude and spatial variability of the change differs in the coastal process-resolving downscaled projections and to a varying degree depending on the variable of interest.

Changes in pCO₂ concentrations, Ω , and pH are modified in the downscaled projections relative to the projected global
555 simulation, suggesting downscaled projections are necessary to more accurately project future conditions of these variables. Carbon variables are likely modified by the inclusion of shelf processes including benthic pelagic coupling and sedimentary processing as suggested by the TA and nutrients correlations. The diversity of these projected changes of future ocean conditions emphasizes the need to improve our understanding of mechanisms by which coastal processes interact with these large-scale drivers of change or properly simulate and capture these feedbacks in projections.

560 **Code and Data Availability**

Archived model fields will be available from the library at UConn ([link](#)) upon acceptance of this publication.

Author Contribution

SS, DP, CD formulated the research goals and designed the experiments and analyses. DP and HF carried out the experiments. TK, SS, JN, and CD acquired the financial support for the project that led to its publication. TK managed and
565 coordinated research meetings with the co-authors. DP and EN performed formal analysis of the model fields. DP created the figures which SS helped design. SS and PM developed the 1.5 km simulations alongside the Coastal Modeling Group at UW. CD developed the 12 km simulations. RF and SA collected the data used for model evaluation and assisted in determining how model evaluation would be performed. SS prepared the manuscript with contributions and edits from all co-authors.

570 **Competing Interests**

The authors declare that they have no conflict of interest.

Acknowledgements

This work was supported by funding from the Schwab Charitable Fund made possible by the generosity of Wendy and Eric Schmidt, the Washington Ocean Acidification Center, and the following awarded to C.D.: NSF (OCE-1635632, OCE-
575 1847687, OCE-1419323, OCE-1737282), NOAA (NA15NOS47801-86, NA15NOS47801-92, NA18NOS4780167), California Sea Grant and Ocean Protection Council (R/OPCOAH-1), and Gordon and Betty Moore Foundation (GBMF3775). This publication is partially funded by the Joint Institute for the Study of the Atmosphere and Ocean (JISAO) under NOAA Cooperative Agreement NA15OAR4320063, Contribution No. 2018-0183. RAF and SRA were funded by NOAA/PMEL, the NOAA Ocean Acidification Program, and the former NOAA Global Carbon Cycle Program. We would like to thank Jennifer
580 Sunday for her participation in helpful discussions. The 12km runs were performed on the Cheyenne cluster at NCAR/CISL.

The 1.5-km simulations were performed on the University of Washington Hyak supercomputer system, supported in part by the University of Washington eScience Institute. This is PMEL contribution number 4919.

References

Adams, K. A., Barth, J. A., & Chan, F.: Temporal variability of near-bottom dissolved oxygen during upwelling off central 585 Oregon. *Journal of Geophysical Research: Oceans*, 118(10), 4839–4854. <https://doi.org/10.1002/jgrc.20361>, 2013.

Bakun, A.: Global Climate Change and Intensification of Coastal Ocean Upwelling. *Science*, 247(4939), 198 LP-201. <https://doi.org/10.1126/science.247.4939.198>, 1990.

Alexander, M. A., S. Shin, J. D. Scott, E. Curchitser, and C. Stock, 2020: The Response of the Northwest Atlantic Ocean to Climate Change. *J. Climate*, 33, 405–428, <https://doi.org/10.1175/JCLI-D-19-0117.1>.

590 Bograd, S. J., Castro, C. G., Di Lorenzo, E., Palacios, D. M., Bailey, H., Gilly, W., & Chavez, F. P.: Oxygen declines and the shoaling of the hypoxic boundary in the California Current. *Geophysical Research Letters*, 35(12). <https://doi.org/10.1029/2008GL034185>, 2008.

Bopp, L., Resplandy, L., Orr, J. C., Doney, S. C., Dunne, J. P., Gehlen, M., et al.: Multiple stressors of ocean ecosystems in the 21st century: projections with CMIP5 models. *Biogeosciences*, 10(10), 6225–6245. [https://doi.org/10.5194/bg-10-6225-2013](https://doi.org/10.5194/bg-10-6225-595_2013), 2013.

Breitburg, D., Levin, L. A., Oschlies, A., Grégoire, M., Chavez, F. P., Conley, D. J., et al.: Declining oxygen in the global ocean and coastal waters. *Science*, 359(6371), eaam7240. <https://doi.org/10.1126/science.aam7240>, 2018.

Caldeira, K., & Wickett, M. E.: Anthropogenic carbon and ocean pH. *Nature*, 425, 365. Retrieved from <https://doi.org/10.1038/425365a>, 2003.

600 Cai, W.J., Xu, Y.Y., Feely, R.A. *et al.* Controls on surface water carbonate chemistry along North American ocean margins. *Nat Commun* 11, 2691. <https://doi.org/10.1038/s41467-020-16530-z>, 2020.

Carter, B. R., Feely, R. A., Mecking, S., Cross, J. N., Macdonald, A. M., Siedlecki, S. A., ... Rodgers, K. B.: Two decades of Pacific anthropogenic carbon storage and ocean acidification along Global Ocean Ship-based Hydrographic Investigations Program sections P16 and P02. *Global Biogeochemical Cycles*, 31(2). <https://doi.org/10.1002/2016GB005485>, 2017.

605 Chan, F., Barth, J. A., Lubchenco, J., Kirincich, A., Weeks, H., Peterson, W. T., & Menge, B. A.: Emergence of Anoxia in the California Current Large Marine Ecosystem. *Science*, 319(5865), 920 LP-920. <https://doi.org/10.1126/science.1149016>, 2008.

Chavez, F.P., Pennington, J.T. , Michisaki, R.P., Blum, M., Chavez, G.M., Friederich, J., et al.: Climate variability and change: Response of a coastal ocean ecosystem. *Oceanography*, 30(4), 128–145, <https://doi.org/10.5670/oceanog.2017.429>, 2017.

Chen, C.A: Shelf-vs. dissolution-generated alkalinity above the chemical lysocline. *Deep-Sea Research II*, 49, 5365–5375. [https://doi.org/10.1016/S0967-0645\(02\)00196-0](https://doi.org/10.1016/S0967-0645(02)00196-0), 2002.

610 Connolly, T. P., Hickey, B. M., Geier, S. L., & Cochlan, W. P.: Processes influencing seasonal hypoxia in the northern California Current System. *Journal of Geophysical Research: Oceans*, 115(C3). <https://doi.org/10.1029/2009JC005283>, 2010.

Crawford, W. R., & Peña, M. A.: Decadal Trends in Oxygen Concentration in Subsurface Waters of the Northeast Pacific Ocean. *Atmosphere-Ocean*, 54(2), 171–192. <https://doi.org/10.1080/07055900.2016.1158145>, 2016.

615 Davis, K. A., Banas, N. S., Giddings, S. N., Siedlecki, S. A., MacCready, P., Lessard, E. J., et al.: Estuary-enhanced upwelling of marine nutrients fuels coastal productivity in the U.S. Pacific Northwest. *Journal of Geophysical Research: Oceans*, 119(12). <https://doi.org/10.1002/2014JC010248>, 2014.

Deutsch, C., Emerson, S., & Thompson, L.: Physical-biological interactions in North Pacific oxygen variability. *Journal of Geophysical Research: Oceans*, 111(C9). <https://doi.org/10.1029/2005JC003179>, 2006.

620 Deutsch, C., Brix, H., Ito, T., Frenzel, H., & Thompson, L.: Climate-Forced Variability of Ocean Hypoxia. *Science*, 333(6040), 336 LP-339. <https://doi.org/10.1126/science.1202422>, 2011.

Deutsch, C., Berelson, W., Thunell, R., Weber, T., Tems, C., McManus, J., et al.: Centennial changes in North Pacific anoxia linked to tropical trade winds. *Science*, 345(6197), 665 LP-668. <https://doi.org/10.1126/science.1252332>, 2014.

625 Deutsch, C., Frenzel, H., McWilliams, J.C., Renault, L., Kessouri, F., Howard, E., et al.: Biogeochemical variability in the California Current System, *Progress in Oceanography* <https://doi.org/10.1101/2020.02.10.942565>, 2020.

Diaz, R. J., & Rosenberg, R.: Spreading Dead Zones and Consequences for Marine Ecosystems. *Science*, 321(5891), 926 LP-929. <https://doi.org/10.1126/science.1156401>, 2008.

Doney, S. C., Fabry, V. J., Feely, R. A., & Kleypas, J. A.: Ocean Acidification: The Other CO₂ Problem. *Annual Review of Marine Science*, 1(1), 169–192. <https://doi.org/10.1146/annurev.marine.010908.163834>, 2009.

630 Doney, S. C.: The Growing Human Footprint on Coastal and Open-Ocean Biogeochemistry. *Science*, 328(5985), 1512 LP-1516. <https://doi.org/10.1126/science.1185198>, 2010.

Doney, S. C., Ruckelshaus, M., Emmett Duffy, J., Barry, J. P., Chan, F., English, C. A., et al.: Climate Change Impacts on Marine Ecosystems. *Annual Review of Marine Science*, 4(1), 11–37. <https://doi.org/10.1146/annurev-marine-041911-111611>, 2011.

635 Doney, S. C., D. S. Busch, S. R. Cooley, and K. J. Kroeker.: The impacts of ocean acidification on marine ecosystems and reliant human communities. *Annu. Rev. Environ. Resour.*, 45. doi:10.1146/annurev-environ-012320-083019, 2020.

Dunne, J. P., Sarmiento, J. L., & Gnanadesikan, A.: A synthesis of global particle export from the surface ocean and cycling through the ocean interior and on the seafloor. *Global Biogeochemical Cycles*, 21(4). <https://doi.org/10.1029/2006GB002907>, 2007.

640 Durski, S. M., Barth, J. A., McWilliams, J. C., Frenzel, H., & Deutsch, C.: The influence of variable slope-water characteristics on dissolved oxygen levels in the northern California Current System. *Journal of Geophysical Research: Oceans*, 122(9), 7674–7697. <https://doi.org/10.1002/2017JC013089>, 2017.

Dussin, R., Curchitser, E. N., Stock, C. A., & Van Oostende, N.: Biogeochemical drivers of changing hypoxia in the California Current Ecosystem. *Deep Sea Research Part II: Topical Studies in Oceanography*, 169–170, 104590.

645 <https://doi.org/https://doi.org/10.1016/j.dsr2.2019.05.013>, 2019.

Fassbender, A. J., Sabine, C. L., Feely, R. A., Langdon, C., & Mordy, C. W.: Inorganic carbon dynamics during northern California coastal upwelling. *Continental Shelf Research*, 31(11), 1180–1192. <https://doi.org/https://doi.org/10.1016/j.csr.2011.04.006>, 2011.

650 Feely, R. A., Okazaki, R. R., Cai, W.-J., Bednaršek, N., Alin, S. R., Byrne, R. H., & Fassbender, A.: The combined effects of acidification and hypoxia on pH and aragonite saturation in the coastal waters of the California current ecosystem and the northern Gulf of Mexico. *Continental Shelf Research*, 152, 50–60. <https://doi.org/https://doi.org/10.1016/j.csr.2017.11.002>, 2018.

Feely, R.A., S. Alin, B. Carter, N. Bednaršek, B. Hales, F. Chan, et al.: Chemical and biological impacts of ocean acidification along the west coast of North America. *Estuar. Coast. Shelf Sci.*, 183(A), 260–270, doi: 10.1016/j.ecss.2016.08.043, 2016.

655 Feely, R.A., S.C. Doney, and S.R. Cooley: Ocean acidification: Present conditions and future changes in a high-CO₂ world. *Oceanography*, 22(4), 36–47, doi: 10.5670/oceanog.2009.95, 2009.

Feely, R. A., Sabine, C. L., Hernandez-Ayon, J. M., Ianson, D., & Hales, B.: Evidence for Upwelling of Corrosive “Acidified” Water onto the Continental Shelf. *Science*, 320(5882), 1490 LP-1492. Retrieved from <http://science.sciencemag.org/content/320/5882/1490.abstract>, 2008.

660 Feely, R. A., Sabine, C. L., Lee, K., Berelson, W., Kleypas, J., Fabry, V. J., & Millero, F. J.: Impact of Anthropogenic CO₂ on the CaCO₃ System in the Oceans. *Science*, 305(5682), 362 LP-366. <https://doi.org/10.1126/science.1097329>, 2004.

Fennel, K., Wilkin, J., Levin, J., Moisan, J., O'Reilly, J., & Haidvogel, D.: Nitrogen cycling in the Middle Atlantic Bight: Results from a three-dimensional model and implications for the North Atlantic nitrogen budget. *Global Biogeochemical Cycles*, 20(3). <https://doi.org/10.1029/2005GB002456>, 2006.

665 Fennel, K., Wilkin, J., Previdi, M., & Najjar, R.: Denitrification effects on air-sea CO₂ flux in the coastal ocean: Simulations for the northwest North Atlantic. *Geophysical Research Letters*, 35(24). <https://doi.org/10.1029/2008GL036147>, 2008.

Friedlingstein, P., Jones, M. W., O'Sullivan, M., Andrew, R. M., Hauck, J., Peters, G. P., et al.: Global Carbon Budget 2019. *Earth Syst. Sci. Data*, 11, 1783–1838, <https://doi.org/10.5194/essd-11-1783-2019>, 2019.

García-Reyes, M., Sydeman, W. J., Schoeman, D. S., Rykaczewski, R. R., Black, B. A., Smit, A. J., & Bograd, S. J.: Under Pressure: Climate Change, Upwelling, and Eastern Boundary Upwelling Ecosystems . *Frontiers in Marine Science* . Retrieved from <https://www.frontiersin.org/article/10.3389/fmars.2015.00109>, 2015.

670 Gattuso, J.-P., Magnan, A., Billé, R., Cheung, W. W. L., Howes, E. L., Joos, F., ... Turley, C.: Contrasting futures for ocean and society from different anthropogenic CO₂ emissions scenarios. *Science*, 349(6243), aac4722. <https://doi.org/10.1126/science.aac4722>, 2015.

Giddings, S. N., MacCready, P., Hickey, B. M., Banas, N. S., Davis, K. A., Siedlecki, S. A., et al.: Hindcasts of potential harmful algal bloom transport pathways on the Pacific Northwest coast. *Journal of Geophysical Research: Oceans*, 119(4). <https://doi.org/10.1002/2013JC009622>, 2014.

680 Grantham, B. A., Chan, F., Nielsen, K. J., Fox, D. S., Barth, J. A., Huyer, A., et al.: Upwelling-driven nearshore hypoxia signals ecosystem and oceanographic changes in the northeast Pacific. *Nature*, 429, 749. Retrieved from <https://doi.org/10.1038/nature02605>, 2004.

685 Gruber, N., Hauri, C., Lachkar, Z., Loher, D., Frölicher, T. L., & Plattner, G.-K: Rapid Progression of Ocean Acidification in the California Current System. *Science*, 337(6091), 220 LP-223. <https://doi.org/10.1126/science.1216773>, 2012.

690 Hartmann, D.L., A.M.G. Klein Tank, M. Rusticucci, L. Alexander, S. Brönnimann, Y. Charabi, et al.: Observations: Atmosphere and Surface Supplementary Material. In: *Climate Change 2013: The Physical Science Basis. Contribution of Working Group I to the Fifth Assessment Report of the Intergovernmental Panel on Climate Change* (Stocker, T.F., D. Qin, G.-K. Plattner, M. Tignor, S.K. Allen, J. Boschung, A. Nauels, Y. Xia, V. Bex and P.M. Midgley (eds.)). Available from www.climatechange2013.org and www.ipcc.ch, 2013.

Hartnett, H. E., & Devol, A. H.: Role of a strong oxygen-deficient zone in the preservation and degradation of organic matter: a carbon budget for the continental margins of northwest Mexico and Washington State. *Geochimica et Cosmochimica Acta*, 67(2), 247–264. [https://doi.org/https://doi.org/10.1016/S0016-7037\(02\)01076-1](https://doi.org/https://doi.org/10.1016/S0016-7037(02)01076-1), 2003.

695 Hauri, C., Gruber, N., Vogt, M., Doney, S. C., Feely, R. A., Lachkar, Z., et al.: Spatiotemporal variability and long-term trends of ocean acidification in the California Current System. *Biogeosciences*, 10(1), 193–216. <https://doi.org/10.5194/bg-10-193-2013>, 2013.

Howard, E. M., Penn, J. L., Frenzel, H., Seibel, B. A., Bianchi, D., Renault, L., et al.: Climate-driven aerobic habitat loss in the California Current System. *Science Advances*, 6(20), eaay3188. <https://doi.org/10.1126/sciadv.aay3188>, 2020a.

700 Howard, E. M., Frenzel, H., Kessouri, F., Renault, L., Bianchi, D., McWilliams, J. C., & Deutsch, C. Attributing causes of future climate change in the California Current System with multi-model downscaling. *Global Biogeochemical Cycles*, 34, e2020GB006646, <https://doi.org/10.1029/2020GB006646>. 2020b

Ianson, D., Allen, S. E., Moore-Maley, B. L., Johannessen, S. C., and Macdonald, R. W.: Vulnerability of a semienclosed estuarine sea to ocean acidification in contrast with hypoxia, *Geophys. Res. Lett.*, 43, 5793– 5801, doi:[10.1002/2016GL068996](https://doi.org/10.1002/2016GL068996), 2016.

Jacox, M. G., C. A. Edwards, E. L. Hazen, and S. J. Bograd: Coastal upwelling revisited: Ekman, Bakun, and improved upwelling indices for the U.S. west coast, *Journal of Geophysical Research*, doi:10.1029/2018JC014187, 2018.

705 Jiang, L., Carter, B.R., Feely, R.A. et al.: Surface ocean pH and buffer capacity: past, present and future. *Sci Rep* 9, 18624. <https://doi.org/10.1038/s41598-019-55039-4>, 2019.

Kwiatkowski, L., & Orr, J. C.: Diverging seasonal extremes for ocean acidification during the twenty-first century. *Nature Climate Change*, 8(2), 141–145. <https://doi.org/10.1038/s41558-017-0054-0>, 2018.

710 Laruelle, G. G., Cai, W.-J., Hu, X., Gruber, N., Mackenzie, F. T., & Regnier, P.: Continental shelves as a variable but increasing global sink for atmospheric carbon dioxide. *Nature Communications*, 9(1), 454. <https://doi.org/10.1038/s41467-017-02738-z>, 2018.

Le Quéré, C., Andrew, R. M., Friedlingstein, P., Sitch, S., Pongratz, J., Manning, A. C., ... Zhu, D.: Global Carbon Budget 2017. *Earth System Science Data*, 10(1), 405–448. <https://doi.org/10.5194/essd-10-405-2018>, 2018.

Lewis, E., and D. W. R. Wallace.: Program Developed for CO₂ System Calculations. ORNL/CDIAC-105. Carbon Dioxide Information Analysis Center, Oak Ridge National Laboratory, U.S. Department of Energy, Oak Ridge, Tennessee.

Li, C., Huang, J., Ding, L., Liu, X., Yu, H., & Huang, J.. (2020). Increasing escape of oxygen from oceans under climate change. *Geophysical Research Letters*, 47, e2019GL086345. <https://doi.org/10.1029/2019GL086345>, 1998.

Liang, J.-H., Deutsch, C., McWilliams, J. C., Baschek, B., Sullivan, P. P., & Chiba, D.: Parameterizing bubble-mediated air-sea gas exchange and its effect on ocean ventilation. *Global Biogeochemical Cycles*, 27(3), 894–905.

<https://doi.org/10.1002/gbc.20080>, 2013.

Lima, F. P., & Wethey, D. S.: Three decades of high-resolution coastal sea surface temperatures reveal more than warming. *Nature Communications*, 3, 704. Retrieved from <https://doi.org/10.1038/ncomms1713>, 2012.

Long, M. C., C. Deutsch, and T. Ito: Finding forced trends in oceanic oxygen, *Global Biogeochem. Cycles*, 30, 381–397, doi:10.1002/2015GB005310, 2016.

Marshall, K. N., Kaplan, I. C., Hodgson, E. E., Hermann, A., Busch, D. S., McElhany, P., et al.: Risks of ocean acidification in the California Current food web and fisheries: ecosystem model projections. *Global Change Biology*, 23(4), 1525–1539. <https://doi.org/10.1111/gcb.13594>, 2017.

Moore, J. K., Doney, S. C., & Lindsay, K.: Upper ocean ecosystem dynamics and iron cycling in a global three-dimensional model. *Global Biogeochemical Cycles*, 18(4). <https://doi.org/10.1029/2004GB002220>, 2004.

Moriarty, J. M., Harris, C. K., Friedrichs, M. A. M., Fennel, K., & Xu, K.: Impact of Seabed Resuspension on Oxygen and Nitrogen Dynamics in the Northern Gulf of Mexico: A Numerical Modeling Study. *Journal of Geophysical Research: Oceans*, 123(10), 7237–7263. <https://doi.org/10.1029/2018JC013950>, 2018.

Morrison, J., Quick, M.C., Foreman, M.G.G.: Climate change in the Fraser River water-shed: flow and temperature projections. *J. Hydrol.* 263, 230–244, 2002.

Orr, J. C., Fabry, V. J., Aumont, O., Bopp, L., Doney, S. C., Feely, R. A., et al.: Anthropogenic ocean acidification over the twenty-first century and its impact on calcifying organisms. *Nature*, 437, 681. Retrieved from <https://doi.org/10.1038/nature04095>, 2005.

Osborne, E.B., Thunell, R.C., Gruber, N. et al.: Decadal variability in twentieth-century ocean acidification in the California Current Ecosystem. *Nat. Geosci.* 13, 43–49 <https://doi.org/10.1038/s41561-019-0499-z>, 2020.

Oschlies, A., Schulz, K., Riebesell, U., & Schmittner, A.: Simulated 21st century's increase in oceanic suboxia by CO₂-enhanced biotic carbon export. *Global Biogeochemical Cycles*. <https://doi.org/10.1029/2007GB003147>, 2008.

Pierce, S. D., Barth, J. A., Shearman, R. K., & Erofeev, A. Y.: Declining Oxygen in the Northeast Pacific. *Journal of Physical Oceanography*, 42(3), 495–501. <https://doi.org/10.1175/JPO-D-11-0170.1>, 2012.

Pilcher, D. J., Siedlecki, S. A., Hermann, A. J., Coyle, K. O., Mathis, J. T., & Evans, W.: Simulated Impact of Glacial Runoff on CO₂ Uptake in the Gulf of Alaska. *Geophysical Research Letters*, 45(2). <https://doi.org/10.1002/2017GL075910>

Pörtner, H. O., & Knust, R. (2007). Climate Change Affects Marine Fishes Through the Oxygen Limitation of Thermal Tolerance. *Science*, 315(5808), 95 LP-97. <https://doi.org/10.1126/science.1135471>, 2018.

Pörtner, H. O., Langenbuch, M., & Reipschläger, A.: Biological Impact of Elevated Ocean CO₂ Concentrations: Lessons from Animal Physiology and Earth History. *Journal of Oceanography*, 60(4), 705–718. <https://doi.org/10.1007/s10872-004-5763-0>, 2004.

750 Qi, D., Chen, L., Chen, B., Gao, Z., Zhong, W., Feely, R. A., et al.: Increase in acidifying water in the western Arctic Ocean. *Nature Climate Change*, 7, 195. Retrieved from <https://doi.org/10.1038/nclimate3228>, 2017.

Rabalais, N. N., D'Viaz, R. J., Levin, L. A., Turner, R. E., Gilbert, D., & Zhang, J.: Dynamics and distribution of natural and human-caused hypoxia. *Biogeosciences*, 7(2), 585–619. <https://doi.org/10.5194/bg-7-585-2010>, 2010.

755 Riche, O., Johannessen, S.C., and Macdonald, R.W.: Why timing matters in a coastal sea: Trends, variability and tipping points in the Strait of Georgia, *Canada Journal of Marine Systems* 131 36-53, 2014.

Renault, L., Hall, A., & McWilliams, J. C.: Orographic shaping of US West Coast wind profiles during the upwelling season. *Climate dynamics*, 46(1-2), 273-289, 2016.

760 Renault, L., Molemaker, M.J., McWilliams, J.C., & Schepetkin, A.F. (2016). Modulation of wind work by oceanic current interaction with the atmosphere. *Journal of Physical Oceanography*, 46(6), 1685-1704. <https://doi.org/10.1175/JPO-D-15-0232.1>

Renault, L., Deutsch, C., McWilliams, J.C., Frenzel, H., Liang, J-H., & Colas, F. (2016) Partial decoupling of primary productivity from upwelling in the California Current system. *Nature Geoscience* 9, 505-508. <https://doi.org/10.1038/ngeo2722>

765 Renault, L., McWilliams, J.C., & Masson, S. (2017). Satellite observations of imprint of oceanic current on wind stress by air-sea coupling. *Scientific Reports*, 7, 17747. <https://doi.org/10.1038/s41598-017-17939-1>

Renault, L., McWilliams, J.C., & Gula, J. (2018). Dampening of submesoscale currents by air-sea stress coupling in the Californian Upwelling System. *Scientific Reports*, 8, 13388.

770 <https://doi.org/10.1038/s41598-018-31602-3>

Renault, L., McWilliams, J.C., Jousse, A., Deutsch, C., Frenzel, H., Kessouri, F., & Chen, R. (2020). The physical structure and behavior of the California Current System. *Progress in Oceanography*, (in review). Preprint on BioRxiv: <https://www.biorxiv.org/content/10.1101/2020.02.10.942730v1>

775 Rykaczewski, R. R., Dunne, J. P., Sydeman, W. J., García-Reyes, M., Black, B. A., & Bograd, S. J.: Poleward displacement
of coastal upwelling-favorable winds in the ocean's eastern boundary currents through the 21st century. *Geophysical Research
Letters*, 42(15), 6424–6431. <https://doi.org/10.1002/2015GL064694>, 2015.

780 Saba, V. S., Griffies, S. M., Anderson, W. G., Winton, M., Alexander, M. A., Delworth, T. L., et al.: Enhanced warming of
the Northwest Atlantic Ocean under climate change. *Journal of Geophysical Research: Oceans*, 121(1), 118–132.
<https://doi.org/10.1002/2015JC011346>, 2016.

Salisbury, J. E., & Jönsson, B. F.: Rapid warming and salinity changes in the Gulf of Maine alter surface ocean carbonate
parameters and hide ocean acidification. *Biogeochemistry*, 141(3), 401–418. <https://doi.org/10.1007/s10533-018-0505-3>, 2018.

785 Shchepetkin, A. F., & McWilliams, J. C.: The regional oceanic modeling system (ROMS): a split-explicit, free-surface,
topography-following-coordinate oceanic model. *Ocean Modelling*, 9(4), 347–404.
<https://doi.org/https://doi.org/10.1016/j.ocemod.2004.08.002>, 2005.

790 Siedlecki, S. A., Banas, N. S., Davis, K. A., Giddings, S., Hickey, B. M., MacCready, P., et al.: Seasonal and interannual
oxygen variability on the Washington and Oregon continental shelves. *Journal of Geophysical Research: Oceans*, 120(2).
<https://doi.org/10.1002/2014JC010254>, 2015.

Siedlecki, S. A., Pilcher, D. J., Hermann, A. J., Coyle, K., & Mathis, J.: The Importance of Freshwater to Spatial Variability
of Aragonite Saturation State in the Gulf of Alaska. *Journal of Geophysical Research: Oceans*, 122(11).
<https://doi.org/10.1002/2017JC012791>, 2017.

795 Sydeman, W. J., García-Reyes, M., Schoeman, D. S., Rykaczewski, R. R., Thompson, S. A., Black, B. A., & Bograd, S. J.:
Climate change and wind intensification in coastal upwelling ecosystems. *Science*, 345(6192), 77 LP-80.
<https://doi.org/10.1126/science.1251635>, 2014.

L.D. Talley, R.A. Feely, B.M. Sloyan, R. Wanninkhof, M.O. Baringer, J.L. Bullister, C.A. et al.: Changes in Ocean Heat,
Carbon Content, and Ventilation: A Review of the First Decade of GO-SHIP Global Repeat Hydrography, *Annual Review of
Marine Science*, 8:1, 185-215, 2016,

800 Takahashi, T., Sutherland, S. C., Chipman, D. W., Goddard, J. G., Ho, C., Newberger, T., ... Munro, D. R.: Climatological
distributions of pH, pCO₂, total CO₂, alkalinity, and CaCO₃ saturation in the global surface ocean, and temporal changes at
selected locations. *Marine Chemistry*, 164, 95–125. <https://doi.org/https://doi.org/10.1016/j.marchem.2014.06.004>, 2014.

Taylor, K. E., Stouffer, R. J., & Meehl, G. A.: An Overview of CMIP5 and the Experiment Design. *Bulletin of the American
Meteorological Society*, 93(4), 485–498. <https://doi.org/10.1175/BAMS-D-11-00094.1>, 2011.

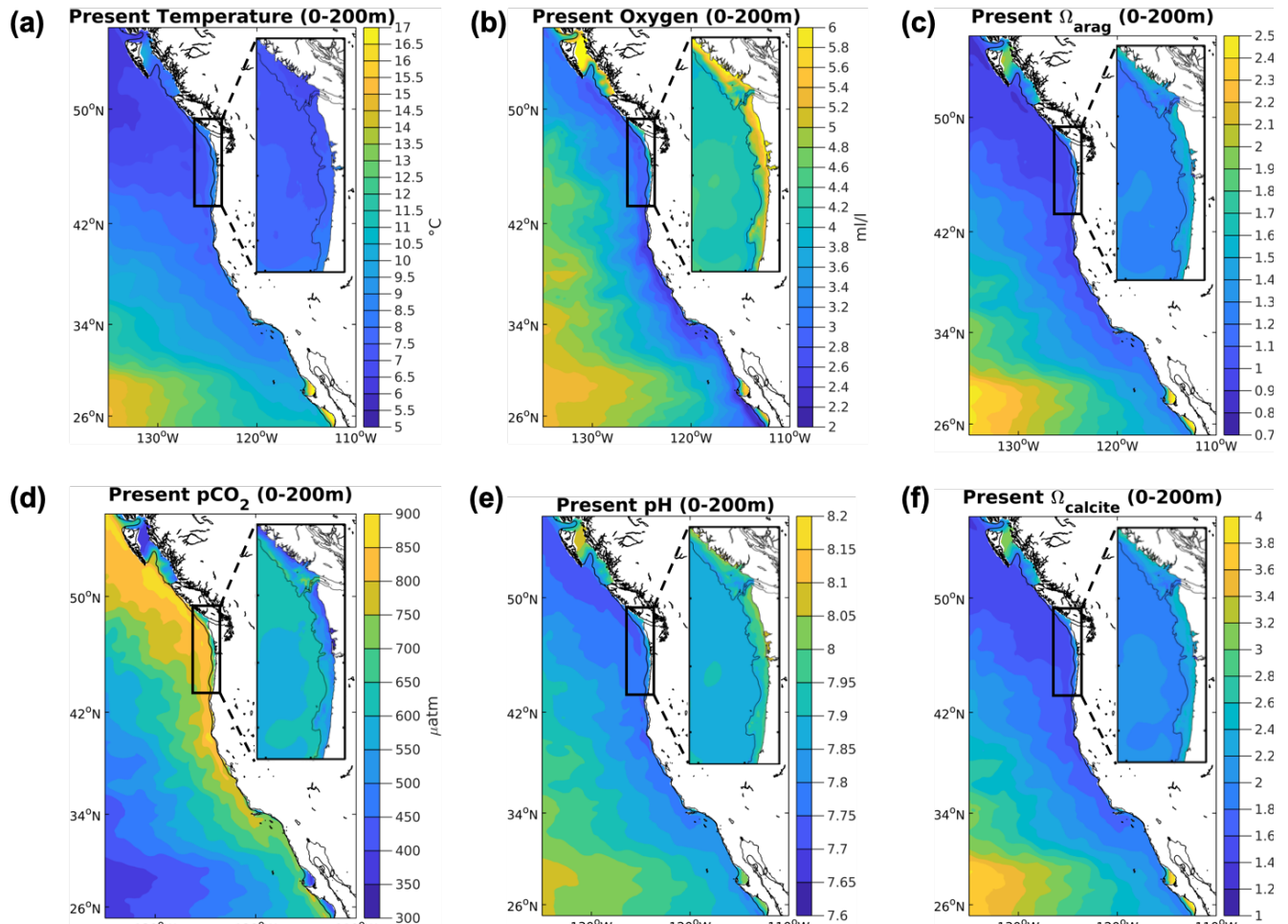
805 Wang, D., Gouhier, T. C., Menge, B. A., & Ganguly, A. R.: Intensification and spatial homogenization of coastal upwelling
under climate change. *Nature*, 518, 390. Retrieved from <https://doi.org/10.1038/nature14235>, 2015.

Xiu, P., Chai, F., Curchitser, E. N., & Castruccio, F. S.: Future changes in coastal upwelling ecosystems with global warming:
The case of the California Current System. *Scientific Reports*, 8(1), 2866. <https://doi.org/10.1038/s41598-018-21247-7>, 2018.

Region	Global	CCS			N-CCS			
Model [Time Interval]; atmospheric CO ₂ (present); atmospheric CO ₂ (future);	A. 1 degree [1971-2000 (present) vs. 2071-2100 (future)]; 326-369 (present); 685-936 (future).	B. 1 degree [1971-2000 (present) vs. 2071-2100 (future)] 346 (present);	C. 12 km [2002-2004 (present) versus 2094-2096 (future)] 372-377 (present); 326-369 (present); 685-936 (future).	D. 12 km Ensemble spread	E. 1 degree [1971-2000 (present) vs. 2071-2100 (future)]; 326-369 (present); 685-936 (future).	F. 12 km [2002-2004 (present) versus 2094-2096 (future)] 372-377 (present); 685-936 (future); 802 (future).	G. 1.5 km [2002-2004 (present) versus 2094-2096 (future)] 371 (present); 800 (future)	H. 12 km Ensemble spread
200m avg								
ΔTemp (°C)	1.97	1.63	1.81, 2.55*	1.38 to 2.24	2.21	1.95, 2.24*	2.32, 2.62*	1.55 to 2.35
ΔOxygen (ml/l)	-0.19	-0.52	-0.62, -0.56*	-0.52 to -0.72	-0.56	-0.72, -0.66*	-0.61, -0.50*	-0.52 to -0.92
ΔpCO ₂ (μatm)	401	492	759, 707*	682 to 836	527	923, 922*	721, 620*	780 to 1066
ΔpH	-0.297	-0.321	-0.333, -0.322*	-0.310 to -0.357	-0.332	-0.315, -0.327*	-0.322, -0.311*	-0.278 to -0.352
ΔΩ _{ang}	-0.85	-0.71	-0.70, -0.68*	-0.65 to -0.75	-0.62	-0.47, -0.53*	-0.58, -0.62*	-0.41 to -0.53
ΔΩ _{calcite}	-1.33	-1.11	-1.11, -1.08*	-1.03 to -1.19	-0.99	-0.74, -0.85*	-0.93, -0.98*	-0.65 to -0.83
Surface								
ΔTemp (°C)	2.49	3.12	3.31, 3.27*	2.57 to 4.05	3.15	3.30, 3.26*	2.89, 2.86*	2.42 to 4.18
ΔOxygen (ml/l)	-0.23	-0.32	-0.35, -0.39*	-0.27 to -0.43	-0.38	-0.41, -0.41*	-0.40, -0.39*	-0.30 to -0.52
ΔpCO ₂ (μatm)	379	392	435, 432*	433 to 437	365	429, 418*	352, 344*	424 to 434
ΔpH	-0.309	-0.319	-0.286, -0.291*	-0.285 to -0.287	-0.343	-0.298, -0.297*	-0.274, -0.271*	-0.296 to -0.300
ΔΩ _{ang}	-0.98	-0.96	-0.90, -0.85*	-0.86 to -0.94	-0.76	-0.85, -0.85*	-0.76, -0.71*	-0.82 to -0.88
ΔΩ _{calcite}	-1.52	-1.50	-1.42, -1.35*	-1.37 to 1.47	-1.21	-1.35, -1.35*	-1.21, -1.14*	-1.30 to -1.40
Bottom (<500m)								
ΔTemp (°C)	1.98	1.65	1.84, 2.33*	1.47 to 2.21	1.34	1.75, 1.90*	2.05, 2.35*	1.40 to 2.10
ΔOxygen (ml/l)	-0.22	-0.43	-0.56, -0.64*	-0.37 to -0.75	-0.63	-0.66, -0.68*	-0.60, -0.60*	-0.40 to -0.92
ΔpCO ₂ (μatm)	432	505	785, 883*	650 to 920	592	965, 1038*	840, 899*	776 to 1154
ΔpH	-0.306	-0.286	-0.259, -0.318*	-0.228 to -0.290	-0.333	-0.271, -0.292*	-0.279, -0.308*	-0.230 to -0.312
ΔΩ _{ang}	-0.68	-0.47	-0.42, -0.59*	-0.38 to 0.46	-0.32	-0.35, -0.38*	-0.43, -0.50*	-0.30 to -0.40
ΔΩ _{calcite}	-1.06	-0.74	-0.66, -0.93*	-0.59 to 0.73	-0.50	-0.56, -0.61*	-0.68, -0.79*	-0.48 to -0.64

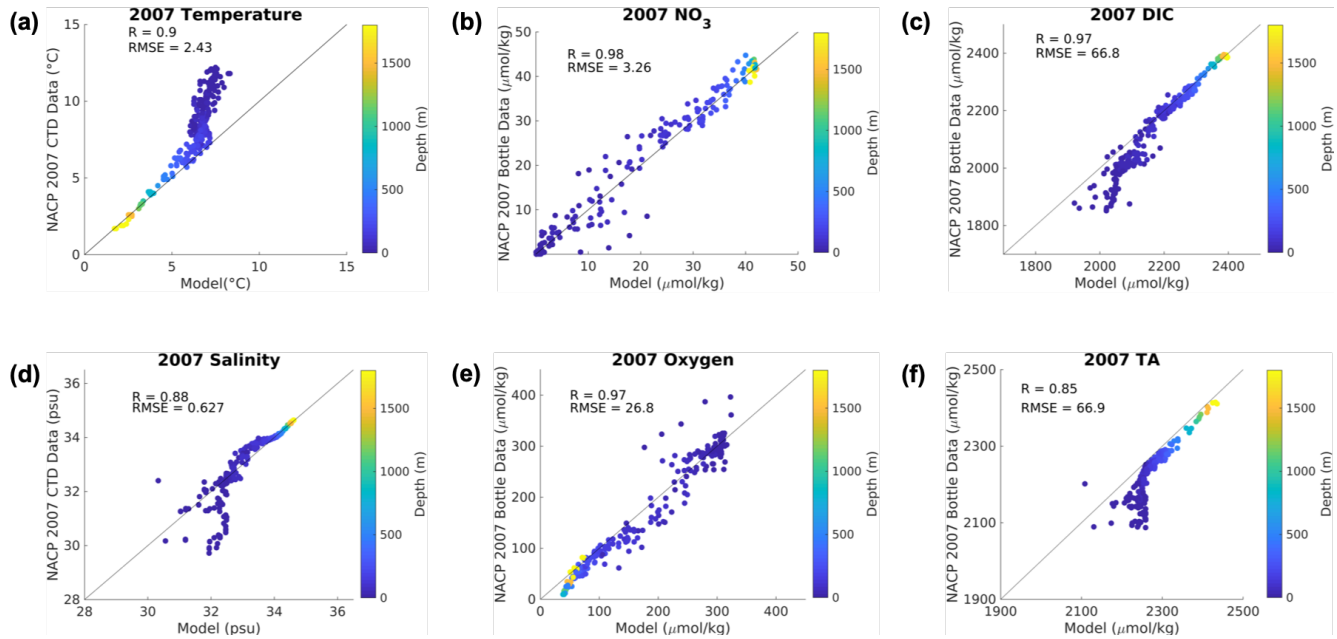
815 **Table 1: Annual average differences between climate stressor variables in the future and the base/modern conditions for the global ensemble, 12-km, and 1.5-km projections over different regions of the water column (200 m averaged, surface, and bottom < 500 m).** Column A depicts the global average from the ensemble average of CMIP5. Column B includes the global (1 degree) ensemble average difference for the CCS region followed by, in column C, the CCS wide difference from the 12km downscaled results. The final CCS column (column D) includes the ensemble spread as the range across the 5-member model spread of the results for the 12-km model projections column for the CCS domain. The N-CCS region results span columns E-H in this table. The next three 820 columns detail the differences in the Cascadia domain for the global ensemble average (column E), the 12-km (column F) and 1.5-km downscaled projections (column G). The final column (column H) includes the ensemble spread as the range across the 5-member model spread of the results for the 12-km model projections column for the Cascadia domain. The direction with which each variable described above was amplified/dampened relative to the global models outside the ensemble variability is highlighted using bold text and dark grey (amplified) and italic text with light grey (dampened) shading. Within the downscaled simulation, values are also provided just on the shelf (< 200 meter isobath) and denoted with an asterisk (*) next to the number.

825

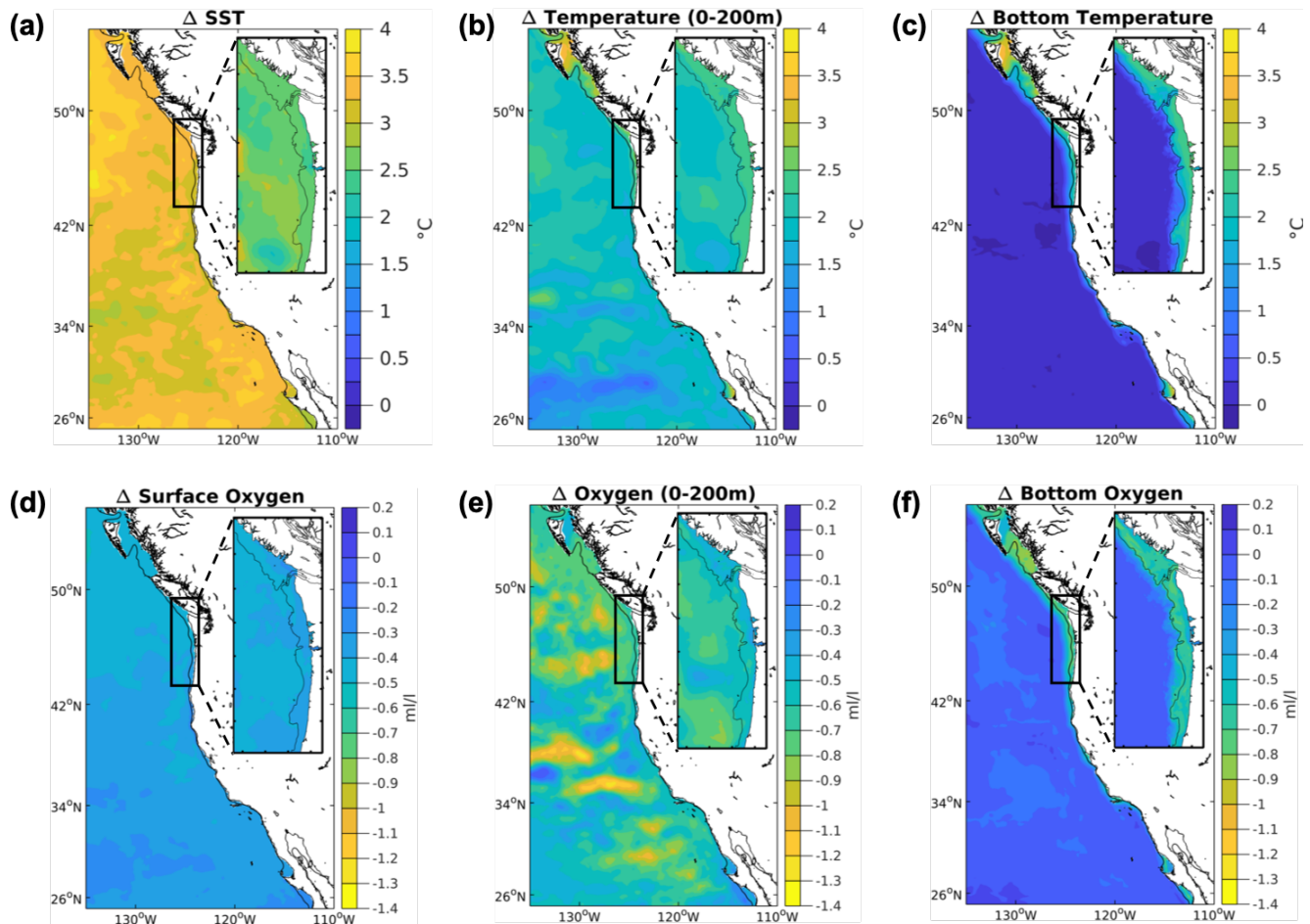


830

Figure 1. Base state climate stressor variables in the CCS in both domains. Depth-averaged over 200 meters values for the climate stressor variables in the base state/modern conditions for the 12-km (CCS-wide, full panel) and 1.5-km simulations (N-CCS, inset) for (a) temperature (deg C) (b) O₂ (ml/l) (c) Ω_{arag} (d) pCO₂ (μatm) (e) pH, and (f) Ω_{calcite} .



835 **Figure 2. Model evaluation.** Comparison between the bottle data from the 2007 cruise detailed in Feely et al. (2008) on the y-axes, and the simulated parameter (x-axis) from the 1.5-km model forced with the 12-km model at the boundaries. Colors indicate the depth where the bottle sample was sampled. Correlation coefficient (R) and Root Mean Squared Error (RMSE) are reported as well. The units for each variable are labeled on the axes.



840 Figure 3. Projected temperature and oxygen changes in the CCS. Differences between climate stressor variables temperature and
 845 oxygen in the future and the base/modern conditions for the 12-km (CCS-wide, full panel) and 1.5-km (N-CCS, inset) projections
 for (a) SST (deg C) (b) depth-averaged temperature over the upper 200 meters (deg C) (c) bottom temperature (deg C) (d) surface
 O₂ (ml/l) (e) depth-averaged O₂ over the upper 200 meters (ml/l) (f) bottom O₂ (ml/l). Positive values indicate a change that is greater
 in the future than the base/present condition and negative values indicate lower values in the future than the base/present conditions
 depicted in Figure 1.

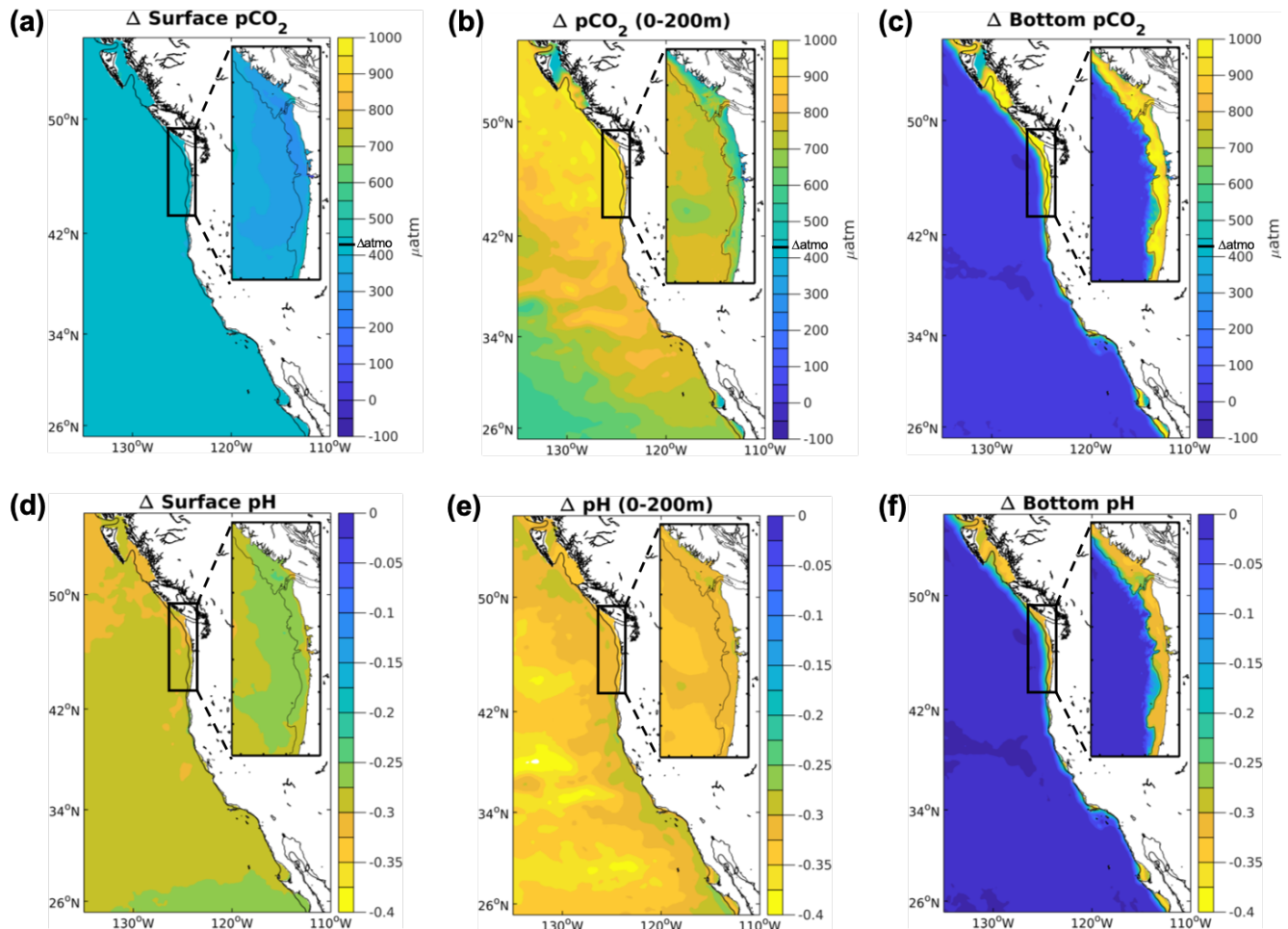


Figure 4. Projected $p\text{CO}_2$ and pH changes in the CCS. Differences between climate stressor variables $p\text{CO}_2$ and pH in the future and the base/modern conditions for the 12-km (CCS-wide, full panel) and 1.5-km (N-CCS, inset) projections for (a) surface $p\text{CO}_2$ (μatm) (b) depth-averaged $p\text{CO}_2$ over the upper 200 meters (μatm) (c) bottom $p\text{CO}_2$ (μatm) (d) surface pH (e) depth-averaged pH over the upper 200 meters and (f) bottom pH. Positive values indicate a change that is greater in the future than the base/present condition and negative values indicate lower values in the future than the base/present condition depicted in Figure 1.

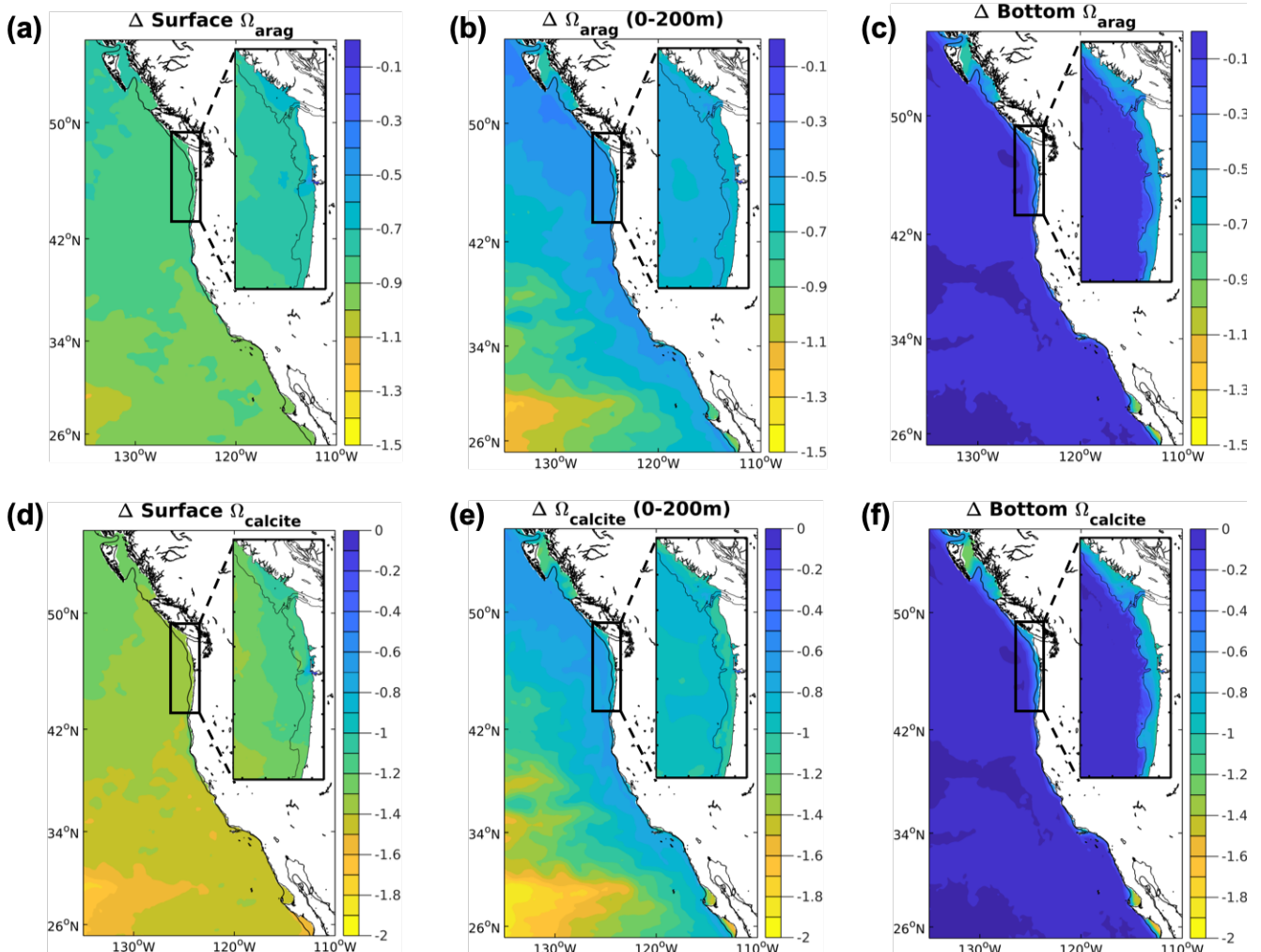


Figure 5. Projected Ω changes in the CCS. Differences between climate stressor variables Ω in the future and the base/modern conditions for the 12-km (CCS-wide, full panel) and 1.5-km projections (N-CCS, inset). (a) surface Ω_{arag} (b) depth-averaged Ω_{arag} over the upper 200 meters (c) bottom Ω_{arag} (d) surface Ω_{calcite} (e) depth-averaged Ω_{calcite} over the upper 200 meters and (f) bottom Ω_{calcite} . Positive values indicate a change that is greater in the future than the base/present condition and negative values indicate lower values in the future than the base/present condition depicted in Figure 1.

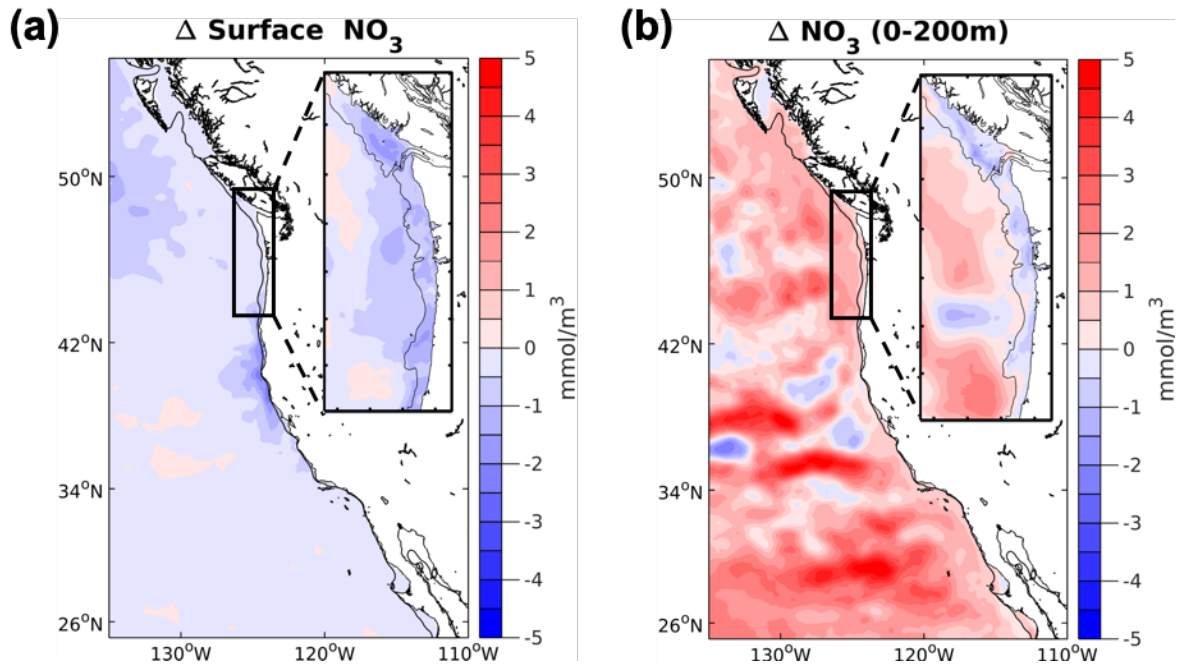
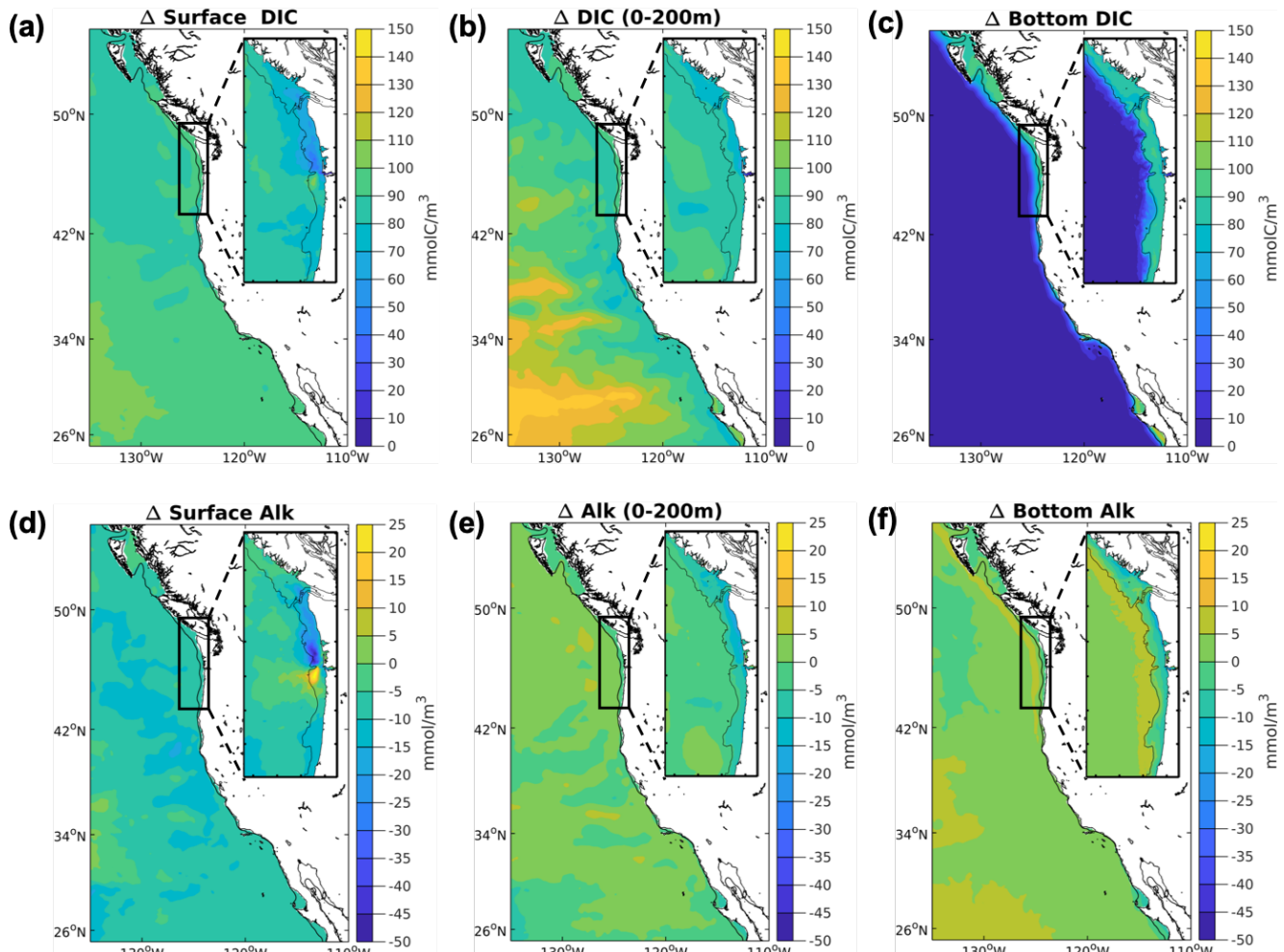


Figure 6. Projected changes in nitrate for the CCS. Differences between the future and the base/modern nitrate (NO_3) conditions for the 12-km (CCS-wide, full panel) and 1.5-km (N-CCS, inset) projections at (a) the surface (b) depth-averaged (0-200m). Positive values indicate a change that is greater in the future than the base/present condition and negative values indicate lower values in the future than the base/present condition.



865 **Figure 7. Projected changes for DIC and TA in the CCS.** Simulated downscaled changes in annual average DIC and TA (mmol/m³) in the future and the base/modern conditions for the 12-km (CCS-wide, full panel) and 1.5-km (N-CCS, inset) projections. (a) Surface DIC (b) 200 m depth averaged DIC (c) bottom DIC (d) Surface TA (e) 200 meter depth averaged TA and (f) Bottom TA. Positive values indicate a change that is greater in the future than the base/present condition and negative values indicate lower values in the future than the base/present condition.